THE USE OF TEMPERATURE AS A GROUND-WATER TRACER IN GLACIAL OUTWASH

by

Paul Martin Barlow

A Thesis Submitted to the Faculty of the

DEPARTMENT OF HYDROLOGY AND WATER RESOURCES

In Partial Fulfillment of the Requirements
For the Degree of

MASTER OF SCIENCE
WITH A MAJOR IN HYDROLOGY

In the Graduate College

THE UNIVERSITY OF ARIZONA

1 9 8 7

STATEMENT BY AUTHOR

This thesis has been submitted in partial fulfillment of requirements for an advanced degree at the University of Arizona and is deposited in the University Library to be made available to borrowers under rules of the Library.

Brief quotations from this thesis are allowable without special permission, provided that accurate acknowledgement of source is made. Requests for permission for extended quotation or reproduction of this manuscript in whole or in part may be granted by the head of the major department or the Dean of the Graduate College when in his or her judgement the proposed use of the material is in the interests of scholarship. In all other instances, however, permission must be obtained from the author.

SIGNED Paul Martin Baker

APPROVAL BY THE THESIS DIRECTOR

This thesis has been approved on the date shown below:

Stanley N. Davis

Stanley N. Davis
Professor of Hydrology and Water Resources

November 25, 1987
Date

TABLE OF CONTENTS

TABLE OF CONTENTS--Continued

LIST OF ILLUSTRATIONS

LIST OF ILLUSTRATIONS--Continued

LIST OF TABLES

To my parents,

Evone and Ralph Barlow,
for their support and encouragement
throughout this project

ACKNOWLEDGMENTS

This thesis would not have been possible without the support in many different capacities of several students and faculty members of the University of Arizona, hydrologists with the U.S. Geological Survey, and my family and friends. To all of these people, I extend a grateful thank you.

Professors Stanley Davis, Jim Yeh, and Eugene Simpson, who comprised my thesis committee, were extremely helpful in the planning of the experiments, interpretation of the results, and in the writing and organization of the thesis. Dr. Davis, my thesis advisor, gave a great deal of support and encouragement throughout the thesis, and provided the initial impetus to carry out the tracer experiment. Dr. Yeh made many helpful suggestions on the analysis of the experimental results, especially on the analysis of longitudinal dispersion. Dr. Simpson also helped in the interpretation of the results and gave insight into the mechanisms of thermal transport.

Support from Denis LeBlanc, Steve Garabedian, and Chip Quadri of the Massachusetts Subdistrict Office of the U.S. Geological Survey was essential to the successful completion of this thesis. All three provided generously of their time and professional judgement as well as labor and materials during the tracer experiment. Their assistance is greatly appreciated.

Wayne Lapham, also of the Massachusetts Subdistrict Office, read the first draft of the thesis and helped me clarify some of my interpretations of the results. Mike Carpenter, of the Tucson Sub-

district Office, aided in the calibration of the thermistors. Charlie Phillips, of the Massachusetts Subdistrict Office, assisted in the collection of field data. Herbert Johnston (Providence), Kenneth Kipp (Denver), and Robert Miller (St. Paul), all of the U.S. Geological Survey, made several suggestions in the early development of the experiment.

Rikki Amutis, of the University of Arizona, assisted in the construction of the field equipment, in the chemical analysis of the samples, in the editing of the thesis, and acted as a sounding board throughout the project. Martin Barackman and Betsy Behl, also of the University of Arizona, gave assistance in the design of the field equipment and in the laboratory analyses, respectively.

The fine typing of the thesis was done by Corla Thies. Beth Johnson and Alex Sololoff drafted some of the figures.

Finally, a hearty thank you to my three volunteer field assistants during the experiment, Rev. A. Ralph Barlow, Andrew Barlow, and Dr. Steve Georas.

ABSTRACT

A twenty-four hour, divergent-flow thermal tracer experiment was conducted to determine the usefulness of heat as a ground-water tracer. Bromide was used also in the experiment, as a means of comparing the thermal tracer to a conservative chemical species. Observations of pore-fluid temperature and bromide concentration were made at seven points within 3.1 meters of a partially-penetrating injection well.

Results show that temperature may be used effectively in the determination of aquifer heterogeneity and aquifer transport and thermal properties. Aquifer porosity was determined to be between 0.35 to 0.61. Longitudinal mass and thermal dispersivities were computed to have been between 0.012 to 0.124 meters, and apparent thermal conductivities were 3.4 to 25.9 times greater than the bulk thermal conductivity of the aquifer. The high conductivities point to the importance of thermal dispersion to the overall transport of a thermal plume during an injection experiment.

CHAPTER ONE

INTRODUCTION

Ground-water tracers, which include any naturally occurring or artificially introduced material or energy within an aquifer, have been used for many years as an aid in the determination of ground-water flow direction and velocity, in the determination of sources of recharge and discharge to aquifers, and in the determination of aquifer hydraulic and transport parameters, including hydraulic conductivity, porosity, and dispersivity. To be successfully employed in a field experiment, the physical and chemical behavior of a ground-water tracer within porous materials must be fully understood (Davis et al., 1985). Although many tracers are currently available which are both non-reactive with the aquifer material and physically well understood, many of these tracers are difficult to sample in the field and analyze in the laboratory, and may pose health hazards to both the hydrologist and communities supplied by the ground water.

Among the potentially useful tracers which currently are not applied often to field studies is heat. Heated or cooled water is well-suited for use as a ground-water tracer because the temperature of water changes slowly as it moves through an aquifer, due to its high heat capacity (Davis et al., 1985). The benefits of the use of heat in ground-water tracer experiments include the simple apparatus needed for its detection, the high degree of sensitivity which may be obtained in the field with inexpensive measuring devices, and the lack of labora-

tory analyses required in its detection. Additionally, heat is environmentally safe.

The drawbacks to the use of heat, or temperature, which is a measure of the heat content of the water, include potential changes brought about to the flow field by the introduction of a plume of water at a different density and viscosity from that of the ambient ground water. Because heat affects the density and viscosity of water, differences in the temperature of injected and ambient waters may lead to a buoyant flow of warm over cold waters, and/or viscous fingering. The hydraulic conductivity of a medium is also a function of the density and viscosity of the pore fluid, and is, therefore, a function of the temperature of the fluid. To avoid significant changes to the flow field and hydraulic conductivity of the medium, temperature contrasts between ambient and traced water must be kept small.

Purpose and Scope of Investigation

This thesis describes the application of heat as a ground-water tracer in glacial outwash deposits of Cape Cod, Massachusetts. A 24-hour, divergent-flow, thermal tracer experiment was conducted to determine the usefulness of heat as a tracer in the outwash material. Bromide, one of the many commonly-used ions in ground-water tracer experiments, was used as a means of comparing the thermal tracer to a conservative chemical tracer. Bromide has been shown to be a conservative chemical species in the aquifer in which the thermal experiments were conducted by Garabedian and others (1987).

The thesis outlines the physical processes which contribute to heat transport, and discusses differences between the transport of heat and a conservative chemical species in porous materials. The design and construction of the temperature-measuring apparatus used in this study are explained in detail, and may serve as a guide in the design of apparatus in future studies. Two small-scale experiments made prior to the 24-hour experiment were conducted to determine the effectiveness of the temperature-measuring apparatus. The results of these experiments are discussed briefly.

During the 24-hour experiment, measurements of pore-water temperature were made, and water samples were collected for the analysis of bromide at seven observation points within 3.1 meters of a partially-penetrating injection well to monitor conditions in the aquifer as thoroughly as possible during the experiment. Measurements of temperature were made in situ, while a peristaltic pump was used to bring water samples to the surface for bromide analysis.

Porosity, longitudinal dispersivity, and bulk and apparent thermal conductivities of the aquifer were estimated from the breakthrough curves to determine if a thermal tracer is a useful means of determining aquifer transport and thermal properties. The effects of the injection temperature of the water used in the experiment on buoyant flow and on the hydraulic conductivity of the aquifer have been examined also, in order to determine as completely as possible the behavior of the tracer in the outwash material.

Previous Investigations

Ground-water temperature has been used in many capacities as a tool in the analysis of subsurface flow systems. Measurements of pore-water temperature have yielded the direction and rate of ground-water flow and have been shown to be effective in determining recharge and discharge areas of aquifers. Temperature measurements have also been used to determine the permeable zones which yield water to pumping wells. Insight on the transport of thermal masses in aquifers has been gained recently from the many aquifer thermal energy storage projects conducted in several countries (a recent review of which is given by Tsang and Hopkins, 1982). The following survey of research papers provides a background on the use of temperature as a naturally occurring and artificially introduced ground-water tracer.

One of the first applications of ground-water thermometry was the determination of vertical recharge rates by the analysis of temperature-depth profiles. Stallman (1963) developed the basic differential equation describing simultaneous heat and water transport in natural material. He showed that temperature measurements could be used to determine ground-water velocity, and in conjuncion with ground-water head measurements could be used to calculate aquifer hydraulic conductivity. Bredehoeft and Papadapulos (1965) later derived a one-dimensional analytical solution to the general equation given by Stallman (1963) and showed how estimates of vertical ground-water velocities could be determined by fitting vertical profiles of groundwater temperature to theoretically-derived type curves.

Sorey (1971) used the solution of Bredehoeft and Papadopulus (1965) to determine vertical flow rates in semi-confining beds in the San Luis Valley of Colorado and the Roswell Basin in New Mexico. Boyle and Saleem (1979) have also determined vertical ground-water velocities and recharge rates to a Silurian dolomite aquifer in northeastern Illinois using temperature-depth profiles in wells. Most recently, Lapham (1987) successfully used temperature profiles and yearly temperature envelopes below stream beds to determine ground-water recharge-discharge velocities and effective vertical hydraulic conductivities of streambed sediments in New England.

Areal studies of ground-water temperature have been made to determine areas of aquifer recharge and discharge. Cartwright (1970) used temperature anomalies throughout the Illinois basin to determine areas in which the discharge of warm water and recharge of cool water occurred. A study in the Tucson basin by Supkow (1971) showed that natural recharge zones were characterized by cool ground water which warmed as it moved through the basin. He also delineated zones of maximum ground-water flow rate, using temperature contours of ground water throughout the basin.

Thermal regimes of ground water have been monitored at pumping wells to determine qualitatively the permeability of individual stratigraphic layers contributing to well discharge (Norris and Spieker, 1962; Schneider, 1972). Keys and Brown (1978) also used temperature logs made at observation points downstream of wells injecting playa lake water to show the vertical variations in hydraulic conductivity in portions of the Ogallala Formation in Texas. Finally, Flynn (1985)

used thermal pulses in low-permeability, fractured granite to identify the location of water-bearing fracture zones between injection and observation boreholes.

CHAPTER TWO

HEAT TRANSPORT IN SATURATED, POROUS MATERIAL

Heat is transported through geologic materials by the processes of radiation, conduction, and convection, which includes the processes of dispersion and buoyant flow. Near an injection well, forced convection is the primary mechanism of heat transport. As a thermal front moves away from the injection well, dispersion and conduction produce a longitudinal and transverse flow of heat away from the center of mass of the thermal plume. Additionally, thermal energy is exchanged by conduction between the heated pore fluid and solid grains of the aquifer's matrix. The grains absorb energy from the heated pore fluid and cause a net retardation in the velocity of the thermal front behind the average movement of the pore fluid. If the difference in density between injected and ambient waters is greater than the horizontal pressure force produced at the injection well, a buoyant flow of the heated, less dense water over the ambient ground water will occur. Heat transfer by radiation takes place also in ground water, but its magnitude is considered to be negligible by researchers and will not be mentioned further.

The discussion which follows focuses on each of the physical processes which contribute to the transport of heat in saturated, porous materials. The differences between the transport of thermal energy and a conservative chemical species are discussed as a reference to the results and analysis of the tracer experiment.

A Mathematical Description of Heat and Mass Transport in Saturated Materials

Equations describing the transport of a non-reactive (conservative) chemical constituent and heat through an aquifer of constant fluid density may be derived by considering the conservation of mass and heat and the laws of Fick and Fourier, respectively. These equations have been summarized by de Marsily (1986) and are listed here for reference to the discussion which follows.

With reference to the velocity of the advancing convective fronts (thermal or chemical), the governing partial differential equations of heat and mass transport are:

Transport of heat

$$\operatorname{div}\left(\frac{\underline{\underline{\lambda}}}{\rho_{aq}\ c_{aq}}\ \operatorname{grad} T\right) - \operatorname{div}\ (\bar{u}*T) = \frac{\partial T}{\partial t} \qquad (2.1)$$

Transport of conservative chemical species

$$\operatorname{div}\ (\underline{\underline{D}}\operatorname{grad} C) - \operatorname{div}\ (\bar{u}C) = \frac{\partial C}{\partial t} \qquad (2.2)$$

where C and T are dimensionless concentration and temperature of the pore fluid:

$$C \text{ or } T = \frac{Z - Z_{min}}{Z_{max} - Z_{min}} \qquad (2.3)$$

where Z = concentration or temperature;

Z_{min} = minimum concentration or temperature in the aquifer; and

Z_{max} = maximum concentration or temperature in the aquifer.

and $\underline{\underline{\lambda}}$ = apparent thermal conductivity tensor;

$\underline{\underline{D}}$ = dispersion tensor;

$\bar{u}^*$ = velocity of the (average) thermal front;

$\bar{u}$ = velocity of the (average) front of a nonsorbing chemical;

ρ_{aq} = density of the solid-fluid medium;

c_{aq} = specific mass heat of the solid-fluid medium; and

t = time.

The first term on the left-hand side of Equations 2.1 and 2.2 describes the mass and thermal flux due to thermal conductive and dispersive transport in the medium, respectively. The second term on the left-hand side of each of the equations describes the convective transport of heat and mass through the porous medium. These transport processes are in balance with the rate of heat, or mass, accumulation or depletion, expressed by the time derivative on the right-hand side of the equations.

The velocities of the advancing thermal and chemical fronts are related to the Darcy velocity, $\bar{U}$, by:

For the thermal front

$$\bar{u}^* = \frac{\rho_f \, c_f}{\rho_{aq} \, c_{aq}} \, \bar{U} \tag{2.4}$$

For the chemical front

$$\bar{u} = \frac{\bar{U}}{\phi} \tag{2.5}$$

where ρ_f = density of the pore fluid;

c_f = specific mass heat of the pore fluid; and

ϕ = total porosity.

and the Darcy velocity is:

$$\bar{U} = - \frac{\underline{\underline{k}}}{\mu} (\text{grad } p + \rho_f g \, \text{grad } z) \tag{2.6}$$

where $\underline{\underline{k}}$ = intrinsic permeability tensor;

μ = dynamic viscosity of the fluid;

p = fluid pressure;

g = acceleration due to gravity;

z = vertical axis directed upward; and

grad z = vector with components (0,0,1).

The thermal and chemical dispersion processes are:

$$\frac{\underline{\underline{\lambda}}}{\rho_{aq} \, c_{aq}} = \frac{\lambda_o}{\rho_{aq} \, c_{aq}} + \underline{\underline{\beta}} \left| \bar{u}^* \right| \tag{2.7}$$

and

$$\underline{\underline{D}} = D_m + \underline{\underline{\alpha}} \left| \bar{u} \right| \tag{2.8}$$

where λ_o = bulk thermal conductivity;

D_m = molecular diffusion coefficient;

$\underline{\underline{\beta}}$ = hydrodynamic thermal dispersivity tensor; and

$\underline{\underline{\alpha}}$ = hydrodynamic mass dispersivity tensor.

Equations 2.1 through 2.8 describe the physical processes which govern the transport of thermal energy and a conservative chemical species in saturated porous materials. Differences in the transport of heat and mass are seen in (1) the conduction and dispersion processes of Equations 2.7 and 2.8, and (2) the exchange of heat between solid and fluid phases, expressed by the ratio of specific volumetric heats of the pore fluid, $\rho_f c_f$, to the specific volumetric heat of the solid-fluid medium, $\rho_{aq} c_{aq}$. The dependence of the Darcy velocity on the pore fluid temperature and concentration of mass is seen in the density and viscosity coefficients of Equation 2.6. In addition to the convective force produced at the injection well, these processes are important in determining the spatial and temporal distribution of heat and mass concentration when water of a different temperature and chemical character than that of the ambient ground water is injected into an aquifer.

Processes of Diffusion, Conduction, and Dispersion

The dispersion tensor for a chemical species (Equation 2.8) consists of the molecular diffusion coefficient, D_m, and hydrodynamic mass dispersion process, $\underline{\underline{\alpha}} \, |\bar{u}|$. The mass dispersivity tensor, $\underline{\underline{\alpha}}$, consists of a component in the direction of flow, longitudinal mass dispersivity, and two components transverse to the flow direction, transverse horizontal dispersivity, and transverse vertical dispersivity. The apparent thermal diffusivity tensor (Equation 2.7) consists of the thermal diffusivity of the porous medium, $\lambda_o/\rho_{aq}c_{aq}$ and the hydrodynamic thermal dispersion of the medium, $\underline{\underline{\beta}} \, |\bar{u}|$. The term $\underline{\underline{\beta}}$ is defined as the thermal dispersivity tensor, consisting of a component in the direction of flow (longitudinal thermal dispersivity), and two components perpendicular to flow (transverse horizontal and transverse vertical thermal dispersivity).

In the absence of ground-water flow, the thermal diffusivity of a porous medium, $\lambda_o/\rho_{aq}c_{aq}$, is much greater than the equivalent molecular diffusion of a solute, D_m. Thermal diffusivities of a sand and gravel aquifer of porosity between 0.25 and 0.50 and a density of solid grains of 2.65 gm/cm^3 lie in the range 10^{-6} m^2/s to 10^{-7} m^2/s (Lunardi, 1981). Molecular diffusion constants for ions in porous materials, however, are of the order of 10^{-9} m^2/s to 10^{-10} m^2/s (de Marsily, 1986; Freeze and Cherry, 1979). These diffusion values, for common ions such as bromide and coarse-grained aquifer materials, indicate that the thermal diffusivity of a porous medium is two to four orders of magnitude greater than the molecular diffusivity of a common ion in the aquifer.

The processes of hydrodynamic thermal dispersion and mass dispersion both result from heterogeneities in aquifer permeability, which cause velocity variations along the path of the advancing thermal and chemical fronts. A distinction between the dispersion of mass and the dispersion of heat is made both for clarity and because there are currently no field experiments to show that the two dispersivity terms, $\underline{\underline{\beta}}$ and $\underline{\underline{\alpha}}$, are asymptotically equal (de Marsily, 1986). Sauty et al. (1979) have reasoned that because the conduction of heat has a stronger effect on the transverse exchange of energy than does the molecular diffusion and transverse dispersion of solutes, the asymptotic (or Fickian) longitudinal hydrodynamic thermal dispersivity should stabilize at a lower value than that of the longitudinal mass dispersivity. However, the only conclusions which may be drawn from the few field experiments conducted to date (summarized in de Marsily, 1986), in which both heat and a chemical species have been used in similarly-designed dispersion experiments, is that the longitudinal thermal dispersivity and longitudinal mass dispersivity are of the same order of magnitude.

Sauty et al. (1979) have found that the thermal conductivity of a porous medium is increased by a factor of 4 to 20 during the injection and withdrawal of heated water, due to thermal dispersion. Field experiments and numerical studies have shown that the recovery efficiency of aquifer thermal energy storage projects may be reduced by the increased dispersion of heat away from the storage zone (Molz et al., 1979; Sauty et al., 1979; Sauty et al., 1982; Tsang and Hopkins, 1982; and Miller, 1984). The thermal dispersivity of a medium is therefore

an important parameter in determining the suitability of an aquifer for thermal energy storage.

In an effort to extend the understanding of thermal dispersion in porous materials and its relationship to mass dispersion, longitudinal mass and thermal dispersivities have been estimated from the chemical and thermal breakthrough curves resulting from the thermal tracer experiment reported here.

Heat Exchange in the Porous Medium

As a thermal plume moves through an aquifer, thermal energy is exchanged between the solid and fluid phases of the medium. Experiments conducted by Houpeurt et al. (1965) have shown that thermal equilibrium between water and sand grains as large as 1 mm (equivalent in size to coarse sand) occurs in less than one minute. Considering this nearly instantaneous thermal equilibrium between solid and fluid phases, heat exchange in a porous medium is analagous to a linear, equilibrium, reversible partitioning of a chemical species between aqueous and solid phases of a porous material (Sauty et al., 1979).

The exchange of heat between fluid and solid phases produces a net retardation in the velocity of the advancing thermal front behind that of the non-reactive chemical front. A mathematical expression describing the displacement of the fronts may be developed by considering Equations 2.4 and 2.5:

Letting

$$\bar{U} = \frac{\rho_{aq} c_{aq}}{\rho_f c_f} \bar{u}^* \qquad (2.9)$$

from Equation 2.4, and

$$\bar{U} = \bar{u}\ \phi \tag{2.10}$$

from Equation 2.5, it is seen that the average fronts, $\bar{u}$ and $\bar{u}^*$, are related by:

$$\bar{u} = \frac{\rho_{aq} c_{aq}}{\phi\ \rho_f c_f}\ \bar{u}^* \tag{2.11}$$

The specific volumetric heat of the aquifer, $\rho_{aq} c_{aq}$, is a function of the volumetric proportions of the fluid and solid phases:

$$\rho_{aq} c_{aq} = \phi \rho_f c_f + (1-\phi)\ \rho_s c_s \tag{2.12}$$

where ρ_s is the density of solid grains and c_s is the specific mass heat of the solid grains (de Marsily, 1986). An expression similar to Equation 2.11, which relates the advancing chemical and thermal fronts, has been developed by Keys and Brown (1978).

The physical parameters controlling the displacement between the two fronts are the densities of the two phases, the specific mass heat of the two phases, and the porosity of the medium. Likely magnitudes of the displacement of the two fronts may be estimated by considering sand and gravel aquifers composed of quartz and feldspars, with porosities varying between 0.25 and 0.50. The specific volumetric heat of quartz and feldspar grains (orthoclase and plagioclase) varies

between about 1.8 and 1.9 x 10^6 J/m^3°C (Birch et al., 1942; Deer et al., 1966), while that of the pore fluid at temperatures between 10 to 30°C is 4.2 x 10^6 J/m^3°C (de Marsily, 1986). It is seen from Equations 2.11 and 2.12 that for a porosity of 0.25, the fronts will be displaced by a factor of 2.1-2.4, while for a porosity of 0.50, the fronts will be displaced by a factor of only 1.4 -1.5. These estimates show that the displacement between the two fronts is decreased with an increase in porosity, since there are fewer solids with which to react.

Equations 2.11 and 2.12 afford a means of determining the porosity of an aquifer if the average time of arrival of heat and mass tracer plumes are measured simultaneously at a point downstream of an injection well, if the thermal and chemical exchanges with adjacent stratigraphic layers are small, and if the specific heats and densities of the two phases of the aquifer are known. The relationship between the average time of arrival of the thermal and chemical fronts has been used in Chapter 6 to estimate aquifer porosity.

Buoyant Flow and Viscosity Effects

The effects of buoyant forces on the movement of an injected plume of water may be examined by considering the average movement of the fluid front (Equation 2.5). The Darcy velocity $\bar{U}$ may be expanded to include a fluid particle of density ρ_f moving within a reference body of ground water with density ρ_o (Bear, 1972). Equation 2.5 may then be written as (Bear, 1972):

$$\bar{u} = - \frac{\underline{\underline{k}}}{\phi\mu} \rho_o \, g \, \text{grad}\left(z + \frac{p}{\rho_o g}\right) - \frac{\underline{\underline{kg}}}{\phi\mu} (\rho_f - \rho_o) \, \text{grad} \, z \qquad (2.13)$$

The movement of the fluid front, Equation 2.13, is then the result of two forces. The first force is the movement due to the piezometric head differences in the flow field, referenced to the ambient fluid of density, ρ_o, and the second is a buoyant force directed vertically upward, arising from the density differences between the injected and ambient fluids (Bear, 1972). The effects of the two forces on the movement of an injected body of water is dependent upon the relative magnitude of the head gradients in the aquifer, or forced convection, to that of the density differences between the two fluids, or free convection (Bear, 1972). Large contrasts in densities between the reference and injected fluids may produce a vertical tilting of the lighter thermal front.

The vertical instability which arises due to density differences may be stabilized by the anisotropy of the permeability tensor and the processes of thermal conduction and dispersion (de Marsily, 1981). Injection of hot water into a porous medium of large horizontal to vertical anisotropy will produce a preferential horizontal movement of the thermal plume, effectively preventing the plume from rising. Vertical thermal conduction and thermal dispersion in the direction of flow will mix the injected and ambient water, decrease the density differences between the two fluids, and diminish the buoyant force as the plume moves away from an injection well. A high concentration of dissolved material may also counterbalance the density differences caused by the contrast in temperatures between injected and ambient water.

Heated water moves more easily than cold water within a porous medium because the viscosity of water decreases with an increase in temperature. An injected plume of hot water may produce an unstable interface between hot and cold waters and induce viscous fingering (de Marsily, 1981). The stability of the interface, however, is a complex phenomenon, dependent upon the densities and viscosities of the two fluids, the permeability of the medium, and the flow velocity (de Marsily, 1986).

Chapter Seven examines the effects of the injection temperature and injection rate on buoyant flow in the area of an injection well, located in a hypothetical aquifer, hydrogeologically similar to the outwash deposits in which the thermal experiment was conducted.

CHAPTER THREE

GEOLOGICAL AND HYDROGEOLOGICAL SETTING

Location and Geological Setting

The thermal tracer experiments were conducted in the glacial outwash deposits of Cape Cod, Massachusetts (Figure 3.1). The outwash deposits are part of the end moraines and outwash plains deposited throughout coastal New York (Long Island), Rhode Island, and Massachusetts during the late Wisconsin age of the Pleistocene (Oldale, 1976).

The outwash material in which the experiments were conducted is part of the Mashpee pitted plain deposits, which consist of well-sorted, fluvially bedded, gravelly sand, and gravel (Oldale, 1981). The Mashpee pitted plain deposits are in the western and central area of the inner Cape, below the Sandwich Moraine and to the east of the Buzzards Bay Moraine (Figure 3.1). The source of the outwash deposits was most likely from the Narragansett Bay-Buzzards Bay and Cape Cod Bay lobes of the retreating ice front; the material was deposited sometime between 15,000 to 14,000 years Before Present (Oldale, 1981a).

The outwash plains of Cape Cod are crossed by streams which derive their flow mostly from ground-water discharge (LeBlanc et al., 1986). The plains are pitted with kettle holes which contain lakes and ponds that commonly intersect the unconfined aquifers of the Cape. Rainfall and snowmelt infiltrate quickly to the ground water because of the high permeability of the outwash deposits (LeBlanc et al., 1986).

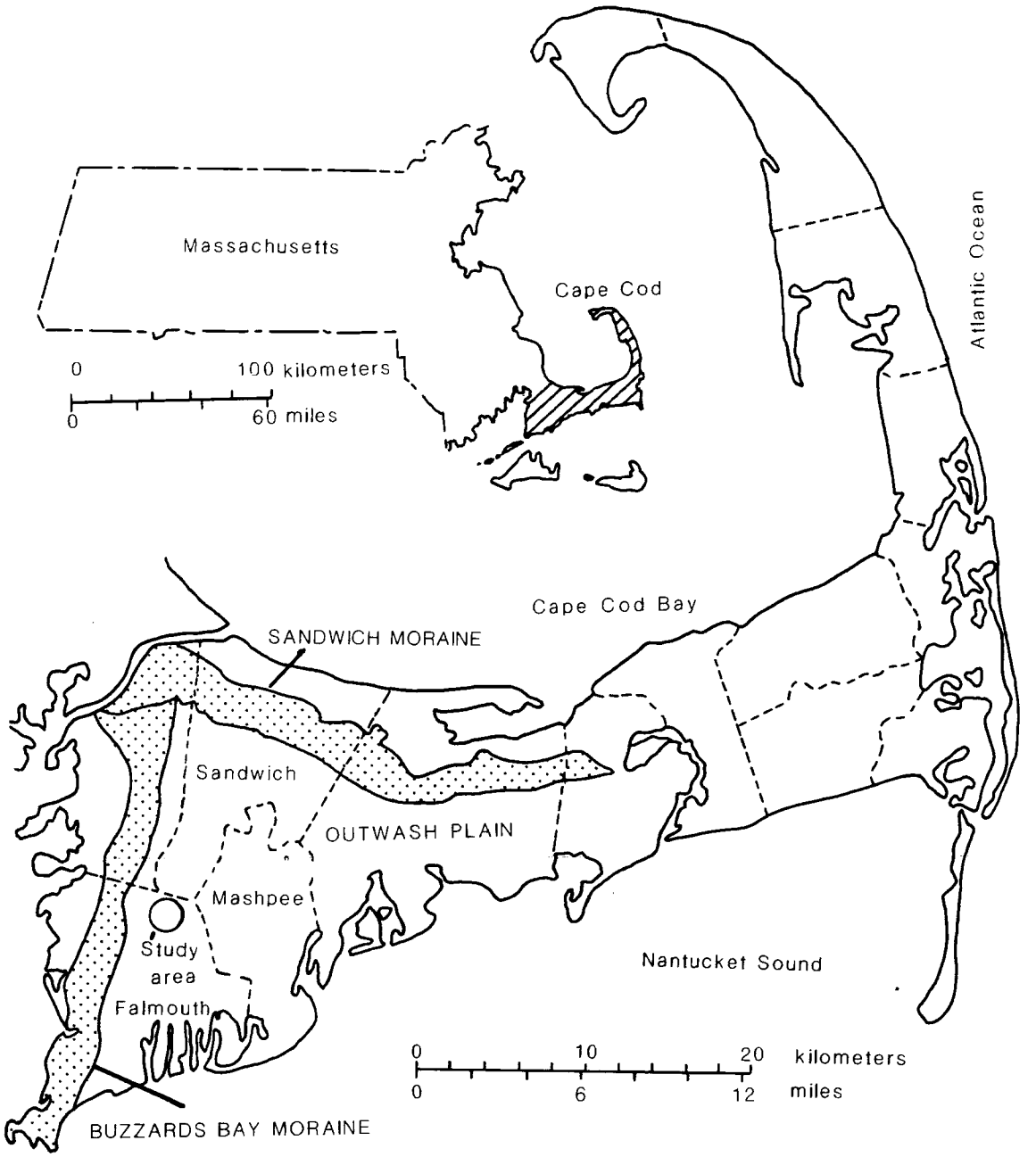

Physical features from Oldale (1976)

Figure 3.1. Geographic setting

Hydrogeology

Detailed hydrogeological research of the aquifer in which the thermal tracer test occurred is being done currently by the United States Geological Survey in conjunction with a large-scale, natural-gradient tracer experiment in the outwash deposits. Much of the following discussion has been drawn from the results of the research conducted at that site, which is approximately 2.2 km from the thermal experiment reported here (Figure 3.2).

The lithology of the aquifer at well FSW-243 (Figure 3.2), drilled approximately 120 m from the thermal tracer test site, consists of fine to coarse sand with a trace of gravel and cobbles, from a depth of 0 to 41.4 meters (0 to 135 feet) below land surface (U. S. Geological Survey files, Boston, Massachusetts). These sands are underlain by at least 5.2 m of fine sand and silty clay at the test site.

Sand and silt size particles account for 90 to 95 percent of the aquifer material at the natural-gradient test site (Barber, 1987). Size analyses of five core samples each 0.3 meters in length and 5 centimeters in diameter (Barber, 1987) show that approximately 18 percent of the material is coarser than 1 mm (millimeter), and that the d_{10} size is approximately 250 microns (0.25 mm). Clays account for less than 0.1 percent of the aquifer material.

Quartz, orthoclase, and plagioclase comprise 90 percent of the sand and silt size fractions, while accessory minerals of igneous and metamorphic origin account for the remaining 10 percent of these materials (Barber, 1987). The percentages of quartz and feldspar increase in the medium to coarse sand size fractions, with only a minor (less

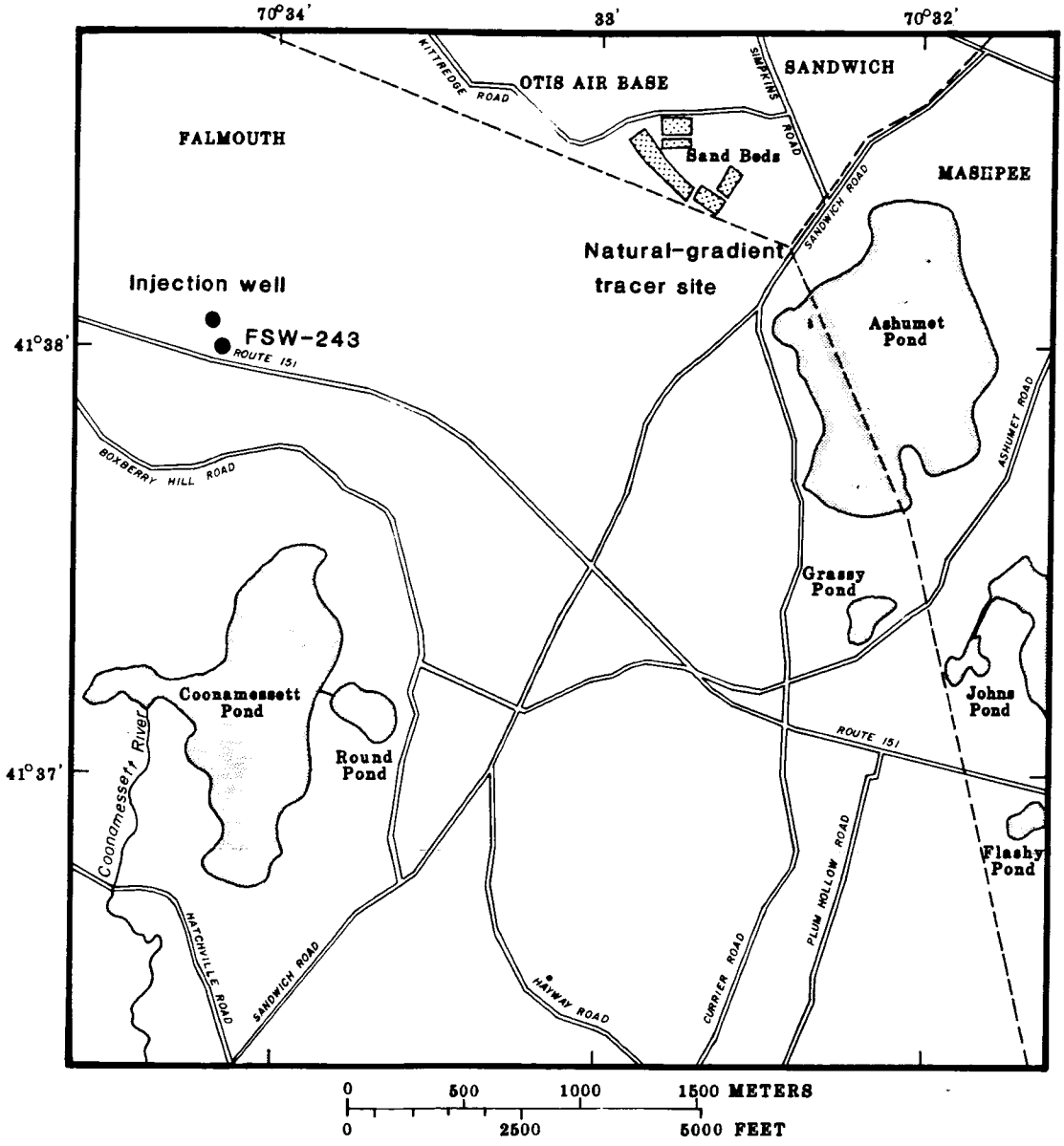

(adapted from LeBlanc, 1984)

Figure 3.2. Location of study area

than five percent) amount of accessory minerals. This mineralogy and particle-size distribution is assumed to be representative of the aquifer material at the thermal tracer site, both because of its proximity to the natural-gradient tracer site and because the two sites lie in the same glacial deposits (Mashpee pitted plain outwash deposits).

Depth to water was 4.8 meters (15.7 feet) below land surface at the injection well (Figure 3.2) prior to the thermal tracer test of August 12, 1986. The water table slopes to the south and southwest at a gradient of .002 and fluctuates seasonally by .3 to 1.0 meter, based on data and information given in LeBlanc (1984). Recharge to the aquifer is estimated to be 53 cm/year (21 in/year), which is 45 percent of average annual precipitation (LeBlanc, 1984) and discharge is to coastal wetlands, streams, and Nantucket Sound to the south (LeBlanc, 1987).

Hydraulic conductivity of the aquifer in the area of the thermal tracer test is highly variable. LeBlanc (1984) used estimates of hydraulic conductivity of sediments on Cape Cod similar to those at the natural-gradient test site and general relationships between grain-size distribution and hydraulic conductivity to estimate hydraulic conductivity at that site to be between 0.07 to 0.11 cm/s. LeBlanc and others (in print) later conducted an aquifer test approximately 2 km southeast of the thermal tracer experiment. Their estimate of hydraulic conductivity based on this test is 0.13 cm/s; their estimate of the ratio of horizontal to vertical hydraulic conductivities is between 2:1 and 5:1.

Hess et al. (1987) have used a multiple-port, constant-head permeameter to measure the hydraulic conductivity of core samples obtained from the natural-gradient tracer site. Their preliminary results have shown a geometric mean of hydraulic conductivity to be 0.024 cm/s at 11°C (the average temperature of the ground water at the natural-gradient tracer site), and an order of magnitude variation around the mean for individual measurements. They have hypothesized that their laboratory-derived hydraulic conductivity values differ from LeBlanc et al. (in print) because of local anisotropy, a true difference in the hydraulic conductivities between the two sites, a scale dependence of the measuring techniques (Hess, LeBlanc, and Wolf, 1987), or a reflection of the small number of samples analyzed to date.

An effective porosity of 38 percent has been determined for the aquifer using a two-well tracer experiment (LeBlanc et al., in print). On the basis of preliminary, uncalibrated neutron logs of wells in the aquifer, LeBlanc et al. (in print) hypothesize that porosity varies only 3 to 5 percent in the outwash material.

Garabedian et al. (1987) have completed a spatial moments analysis of data from the natural-gradient tracer experiment and have estimated an asymptotic longitudinal dispersivity of 0.96 meters. They have estimated transverse horizontal dispersivity to be about 1.8 cm and transverse vertical dispersivity to be about 0.15 cm. Their calculations are based on 17 synoptic observations of the three-dimensional tracer plume, made approximately once every month. As many as 10,000 samples were collected in each monthly sampling round (LeBlanc et al., 1987).

CHAPTER FOUR

EXPERIMENTAL DESIGN AND PROCEDURE

This chapter outlines the construction and calibration of the temperature measuring apparatus, the design and methodology of the thermal tracer experiments, and the methods of analysis of bromide concentrations of the pore fluid.

Temperature Measuring Apparatus

Design

Thermistors were used to measure temperature changes in the aquifer during the tracer experiment. Preliminary field measurements made prior to the 24-hour experiment showed the importance of *in situ* temperature measurements. Using the equipment described below, it was found that temperature measurements made within the aquifer differed as much as 1°C from temperature measurements made at the land surface.

The design of the *in situ* temperature measuring equipment was dictated by the construction of the multi-level samplers at the thermal tracer test site. These multi-level samplers were designed and constructed by Steve Garabedian of the U. S. Geological Survey in Boston, Massachusetts. The multi-level samplers (Figure 4.1) consist of a 3.175 centimeter (1.25-inch) PVC pipe in which 9, 0.4-centimeter (1/6-inch inside diameter) polyethylene sampling tubes tap different levels of the aquifer. The sampling points are spaced 0.3 meters (one foot) apart vertically.

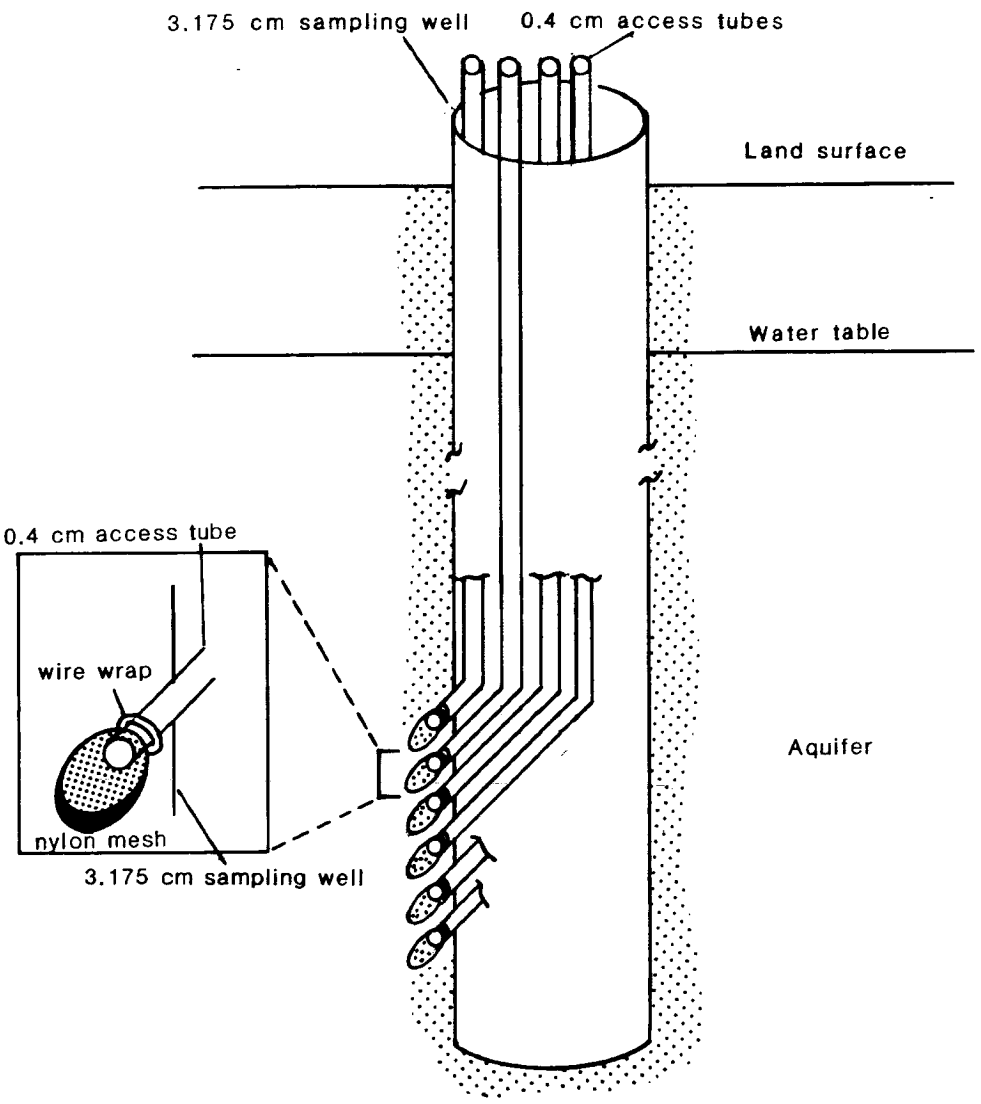

Figure 4.1. Multi-level sampling well

Yellow Springs Instrument 44000 series thermistors were used in the experiments (Figure 4.2). The thermistor bead and #32 tinned copper wire (7.6-cm long) were soldered to 12.8 meters (42 feet) of #28 insulated copper wire. The 12.8 meters of wire were then housed in 0.3-cm (1/8-inch) Eastman Poly-Flo polyethylene tubing, while the termistor bead and approximately 7.6 cm of wire were allowed to project from the tubing. To assure that the soldering points and thermistor bead remained dry during the test, silicon rubber was placed on the tip of the thermistor bead projecting from the Poly-Flo tubing. A banana-plug was then soldered to the land-end of the copper wire to allow attachment to a resistance-reading multimeter (a Keithly 169 multimeter was used in the experiment).

To allow the thermistors to remain in the aquifer throughout the experiment, water samples were pumped through the 0.4-cm access tube around the thermistor apparatus. This was accomplished by placing a plastic T on the land-end of the thermistor apparatus (Figure 4.2). One end of the T was sealed to the 0.4-cm access tube, the opposite end passed the thermistor tubing (which was then attached to the multi-meter), and the mid-opening of the T was attached to the tubing of the peristaltic pump, used to draw water from the sampling points. Silicon rubber was then applied to all ends of the T to seal the pump from the atmosphere.

Calibration

Temperature affects the electrical resistance of the thermistor bead. As the temperature of the medium surrounding the thermistor

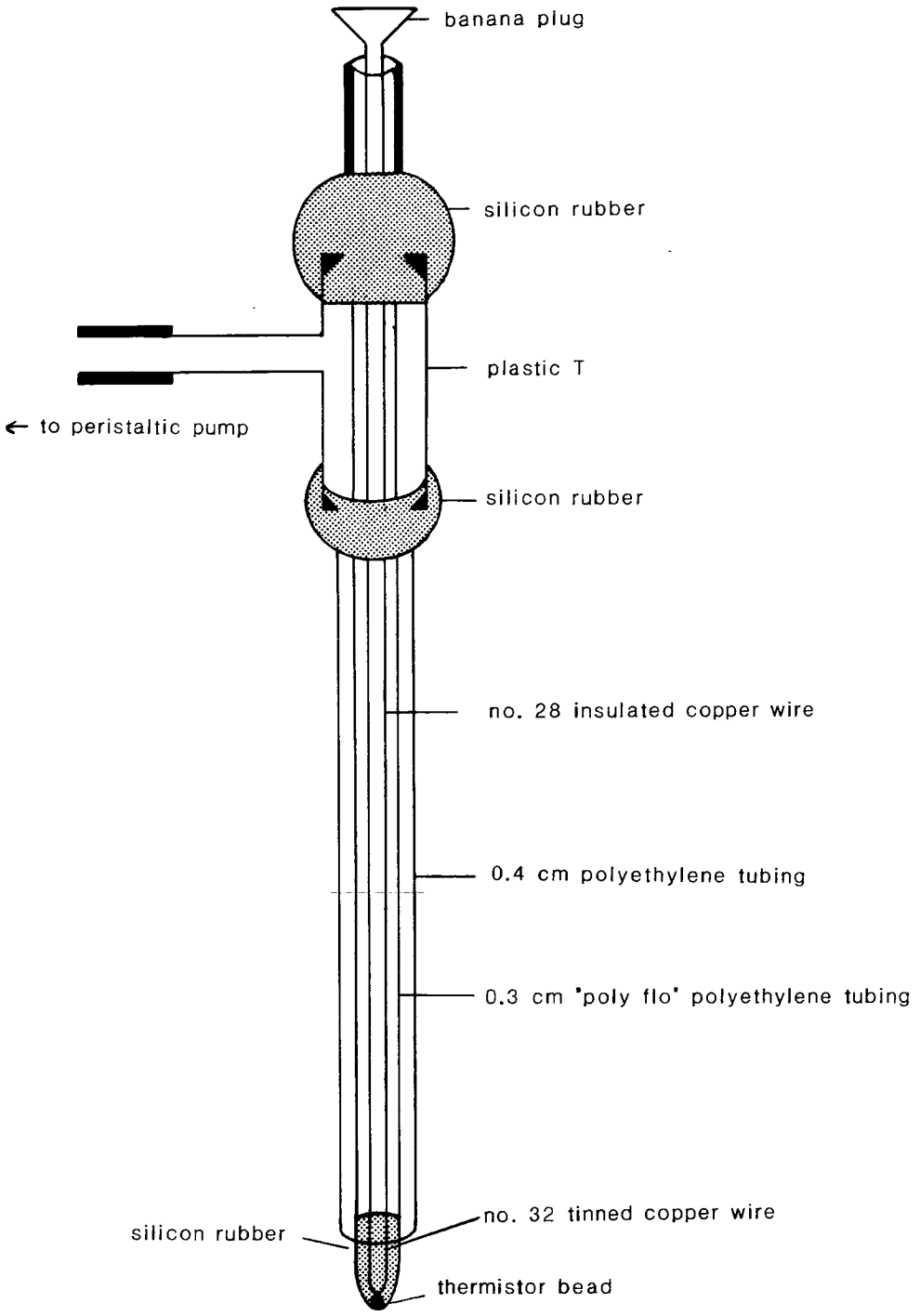

Figure 4.2. Design of temperature-measuring apparatus

rises, the resistance to the flow of current in the bead decreases non-linearly. The Steinhart and Hart equation has been found to be the most reliable method of relating the resistance of the bead to the medium's temperature (Yellow Springs Instrument Company, 1985). The Steinhart and Hart equation is:

$$\frac{1}{T} = a + b(\ln R) + c(\ln R)^3 \qquad (4.1)$$

where:

T = temperature (degrees Kelvin);

R = resistance (ohms); and

a, b, c = constants determined by calibration.

Three water baths at known temperatures are used to determine the coefficients a, b, and c. Calibration of the thermistors used in this experiment was done against thermometers with an accuracy of +/-0.01°C (Brooklyn Thermometer Co., Serial Numbers 307 and D7363). The temperature of the calibration baths, the resistances measured for each of the thermistors during calibration, and the calculated coefficients, a, b, and c, for each thermistor are listed in Appendix A, Tables A-1 and A-2. Although the calibrations were made using a 4-digit multimeter (at the U. S. Geological Survey in Tucson, Arizona), a 3-digit multimeter was used in the experiment. This reduced the precision of the temperature measurements to approximately +/-0.02°C.

Small-scale Thermal Experiments: Design and Methodology

Two small-scale experiments were conducted prior to the 24-hour experiment to test the effectiveness of the equipment and temperature sampling technique described in the preceeding section. The results of these two experiments are discussed briefly in Chapter Five.

Injection and Sampling Configuration

In these small-scale experiments, hot water was injected into the aquifer through one of the 0.4-cm access tubes of the multi-level samplers. Temperature changes over time were then measured above and below this injection point, at the same multi-level sampler (Figure 4.3). Bromide was not used as a tracer in these experiments.

The first test was conducted on March 18, 1986, at the natural-gradient test site. The design of the wells at this site is similar to the design of wells at the thermal tracer site. The only difference is that the spacing between sampling points in the aquifer is 25.4 cm (10 inches at the natural-gradient tracer site, as opposed to 30.5 cm (one foot) at the thermal test site. Monitoring of pore-water temperature was done at points 25.4 cm above and 25.4 cm below the injection point (Figure 4.3).

The second small test was conducted at the thermal tracer site on August 2, 1986. Monitoring of temperature changes in the aquifer was done at points 30.5 cm and 61 cm (two feet) above the injection point, and 30.5 cm and 61 cm below the injection point (Figure 4.3).

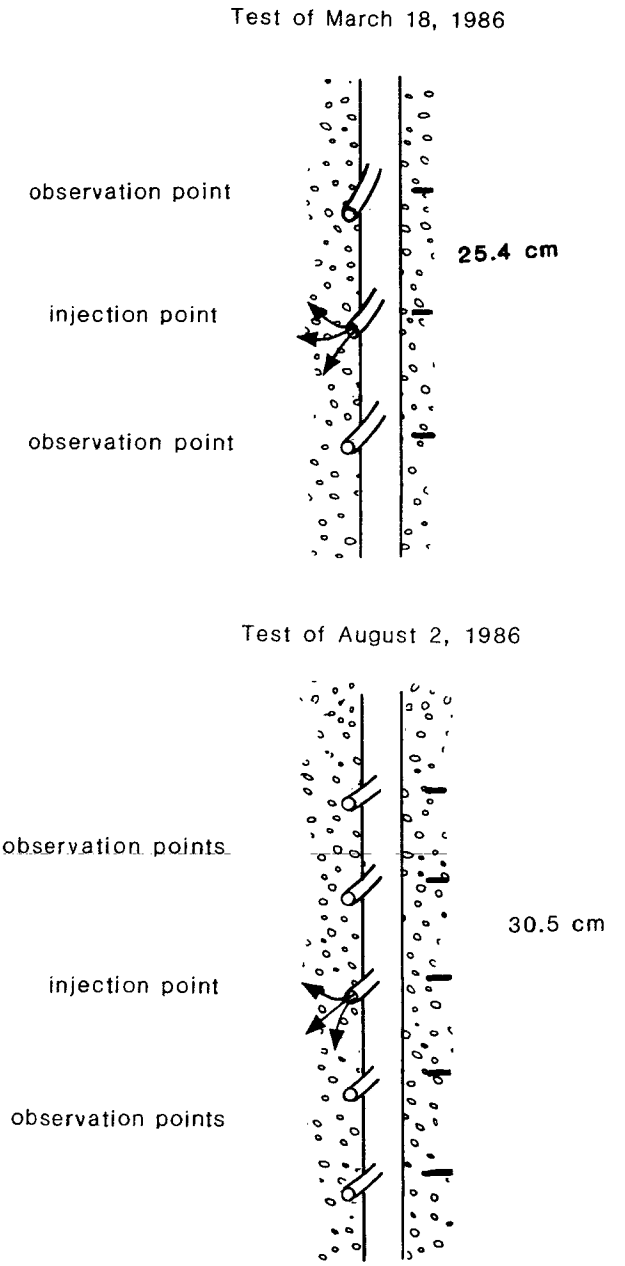

Figure 4.3. Injection configuration for small-scale experiments

Flow Rate and Volume of Water Injected

In the small-scale experiments, hot water was transported from Otis Air Base (0.8 km north of the thermal tracer test site) in 0.1 m^3 (25-gallon) plastic garbage cans.

The test of March 18, 1986, consisted of injecting approximately 95 liters (25 gallons) of hot water at a temperature of 26.5°C, followed by 64 liters (17 gallons) of cold water at 12.0°C. A Geopump 2 peristaltic pump was used to inject water through the 0.4-cm injection (access) tube. Injection was maintained at an average rate of 1.5 liters per minute. Flow rate was measured by determining the length of time required for the pump to drain 250 milliliter sample bottles.

The test of August 2, 1986, consisted of injecting approximately 265 liters (70 gallons) of water at an average temperature of 39.0°C, followed by 64 liters of water at an average temperature of 10.0°C. A Geopump 2 peristaltic pump was again used, and injection was maintained at an average rate of 1.1 liters per minute.

24-hour Tracer Test Design and Methodology

Well Configuration

The 24-hour experiment utilized an injection well screened from 10.1 to 11.3 meters (33 to 37 feet) below land surface, or 5.3 to 6.5 meters (17.3 to 21.3 feet) below the water table prior to the experiment of August 12, 1986. Injected water was pumped from a supply well located 91 meters from the injection well (Figure 4.4). Monitoring of thermal and chemical concentrations of the pore fluid was done at two multi-level sampling wells located 1.7 meters (well 5ab) and 3.1 meters

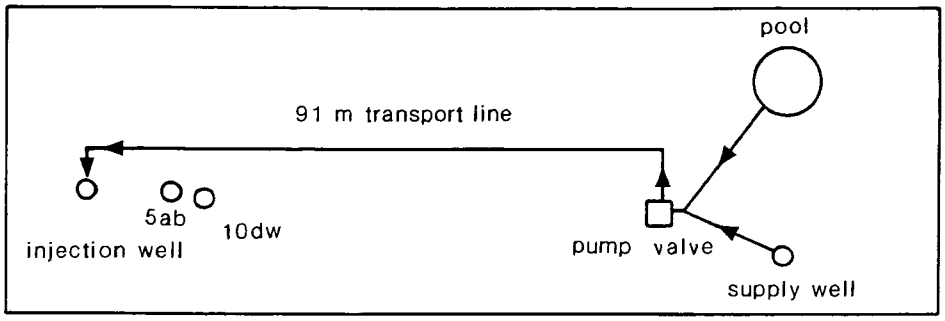

Plan view. Not to scale.

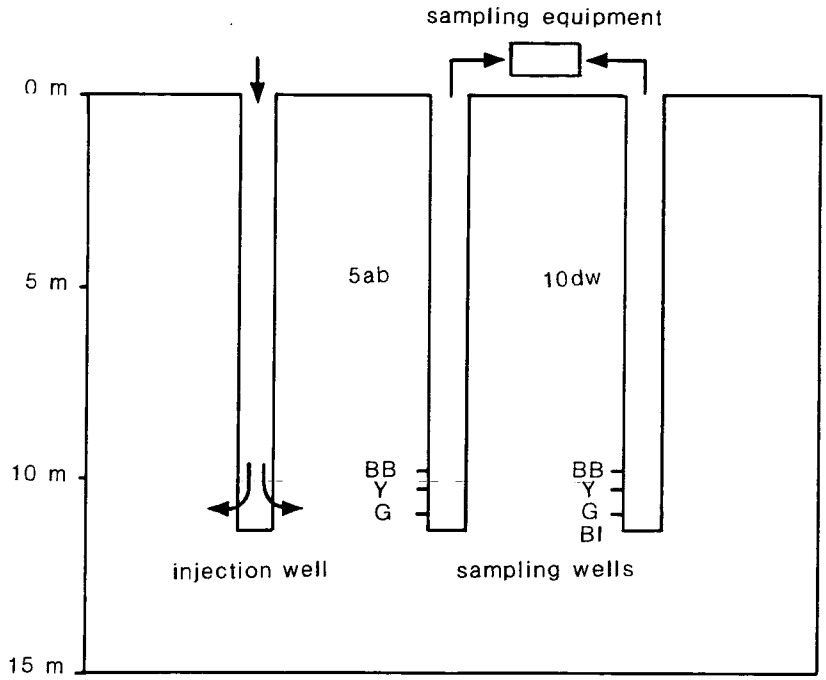

Cross-sectional view.

Figure 4.4. Divergent-flow, thermal tracer experiment design

(well 10dw) from the injection well. Details of the construction of the injection well and multi-level sampling wells are given in Appendix B. Sampling of the aquifer pore fluid was done at a total of seven locations. These locations are (Figure 4.4):

Well 5ab, 1.7 meters from the injection well:

5ab-bb	10.4 m (34 feet) below land surface
5ab-y	10.7 m (35 feet) below land surface
5ab-g	11.3 m (37 feet) below land surface

Well 10dw, 3.1 meters from the injection well:

10dw-bb	10.4 m (34 feet) below land surface
10dw-y	10.7 m (35 feet) below land surface
10dw-g	11.3 m (37 feet) below land surface
10dw-bl	11.9 m (39 feet) below land surface

These intervals were chosen to obtain the most complete vertical sampling of aquifer temperature and bromide concentration during the tracer experiment. Measurements had been planned to be made at a sampling point either 9.5 m or 9.8 m below land surface; however, the walls of the 0.4-cm access tubes which sampled these intervals were too thick to allow passage of the thermistor apparatus.

Preparation of Tracer Solution

A 3.7 m diameter (12-foot) children's pool was used to prepare the tracer solution for injection. A total of 3,450 liters of water

with an in-ground temperature of 9.7°C were pumped from the supply well to the pool. The flow rate into the pool was measured using an orifice-plate flowmeter (RCM Industries). The flowmeter is designed to regulate flows between 19 and 190 liters (5 and 50 gallons) per minute and has an accuracy of at least 10 percent. To this were added approximately 2,270 liters of hot water with a temperature of about 65°C. The hot water was obtained from Otis Air Base and transported to the test site in a 3.8 m^3 (1000-gallon) Army water truck. Spot measurements of temperature in the pool were made prior to the 24-hour experiment. Pool water varied in temperature from 31° to 35°C.

Bromide, in the form of sodium bromide, was used as the conservative tracer in the 24-hour experiment. Three samples of the pool water taken prior to injection of the tracer solution were analyzed using a Dionex ion chromatograph at the University of Arizona. These samples had bromide concentrations of 170 mg/l, 173 mg/l, and 176 mg/l, which indicates that the pool had been well-mixed prior to the start of the experiment. Mean concentration of the pool was, therefore, 173 mg/l. Concentrations of bromide in the aquifer prior to the test were 0.1 mg/l.

Flow Regulation and Sequence of Injection

Water was injected at the rate of 95 liters (25 gallons) per minute during the 24-hour experiment. The flow rate into the injection well was measured using the orifice-plate flowmeter. The water was transported from either the supply well or pool through a 3.175-cm polyethylene tube, 91 m in length, to the injection well (Figure 4.4).

A gasoline-powered pump with a three-way valve was used to pump the water through the transport line. The sequence of injection was as follows:

(1) Ground water from the supply well was injected at the injection well for 45 minutes, to develop the radially-divergent flow field;

(2) The pump valve was switched immediately to a short piece (approximately 9 meters) of 3.175-cm polyethylene line connected to the pool, and the tracer solution was injected for 59 minutes and 30 seconds; finally,

(3) The pump valve was switched back to the supply well line, and ground water was injected into the aquifer for another 22 hours and 15 minutes.

Bromide Sampling and Temperature Measurements

Bromide samples were collected at the seven sampling intervals by pumping water samples to the surface with a Geopump 2 peristaltic pump. Samples were collected at a rate of about .5 milliliters per second. Sixty-milliliter samples were collected and brought to the University of Arizona for analysis. At well 5ab, samples were collected at five- and then ten-minute intervals; at well 10dw, sampling times varied from five minutes to one hour.

Temperature measurements could be made almost continuously, although there was only one multimeter and six thermistor devices.

Temperature measurements were made more frequently as the thermal pulse passed each sampling point.

Water was continuously drawn over the temperature apparatus during this experiment. This assured that the in situ temperature measurement was representative of the same water which was withdrawn from the sampling tube for bromide analysis, and that any disturbances brought about by the 5-cm pvc pipe or disturbances to the aquifer material in the construction of the well did not interfere with the temperature distribution in the aquifer.

The temperature of the injected water was also measured throughout the experiment at the screened interval of the injection well. This was accomplished by taping one of the thermistor devices to the 3.175-cm injection line placed in the injection well. These measurements removed any ambiguity as to the temperature of the water injected into the aquifer.

Bromide Analysis

Water samples collected during the experiment were analyzed for bromide using both a Corning bromide specific ion electrode and a Dionex ion chromatograph. Of the 212 samples analyzed, only 64 were analyzed using the ion chromatograph (Appendix C). Although the two analytical techniques yielded bromide concentrations which differed by less than 10 percent in the majority of samples, some measurements differed by as much as 36 percent. The largest differences occurred for samples with a concentration of less than 10 mg/l. The maximum

difference between the two techniques, however, was only 15 percent of the injection concentration (173 mg/l).

CHAPTER FIVE

RESULTS OF THE TEMPERATURE TRACER EXPERIMENTS

This chapter presents a graphical and qualitative summary of the results of the thermal tracer experiments. A quantitative analysis of the breakthrough curves resulting from the 24-hour experiment is given in Chapter Six.

Small-scale Experiments

In the test of March 18, 1986 thermal breakthrough occurred at both observation points, 25.4 cm above and below the injection point (Figure 5.1). The peak temperature measured at the top point was 20.6°C, while for the bottom point, peak temperature was 21.0 °C. The two curves are very similar in shape, implying that buoyant forces were not important to the transport of heat in this test. The variation between the two curves is most likely due to disturbances of the aquifer near the 3.175-cm PVC sampling well or to heterogeneity of the aquifer. Water was not drawn over the thermistors in this experiment, and the 3.175-cm PVC pipe may have absorbed some of the thermal energy.

A total of 95 liters of water was injected into point B (Figure 5.1). If the flow around the injection point was spherical, which would be likely for the point injection of water, and is suggested by the similarity in breakthrough curves, the radius of aquifer through which the injected water would have passed is 39.1 cm, ignoring disper-

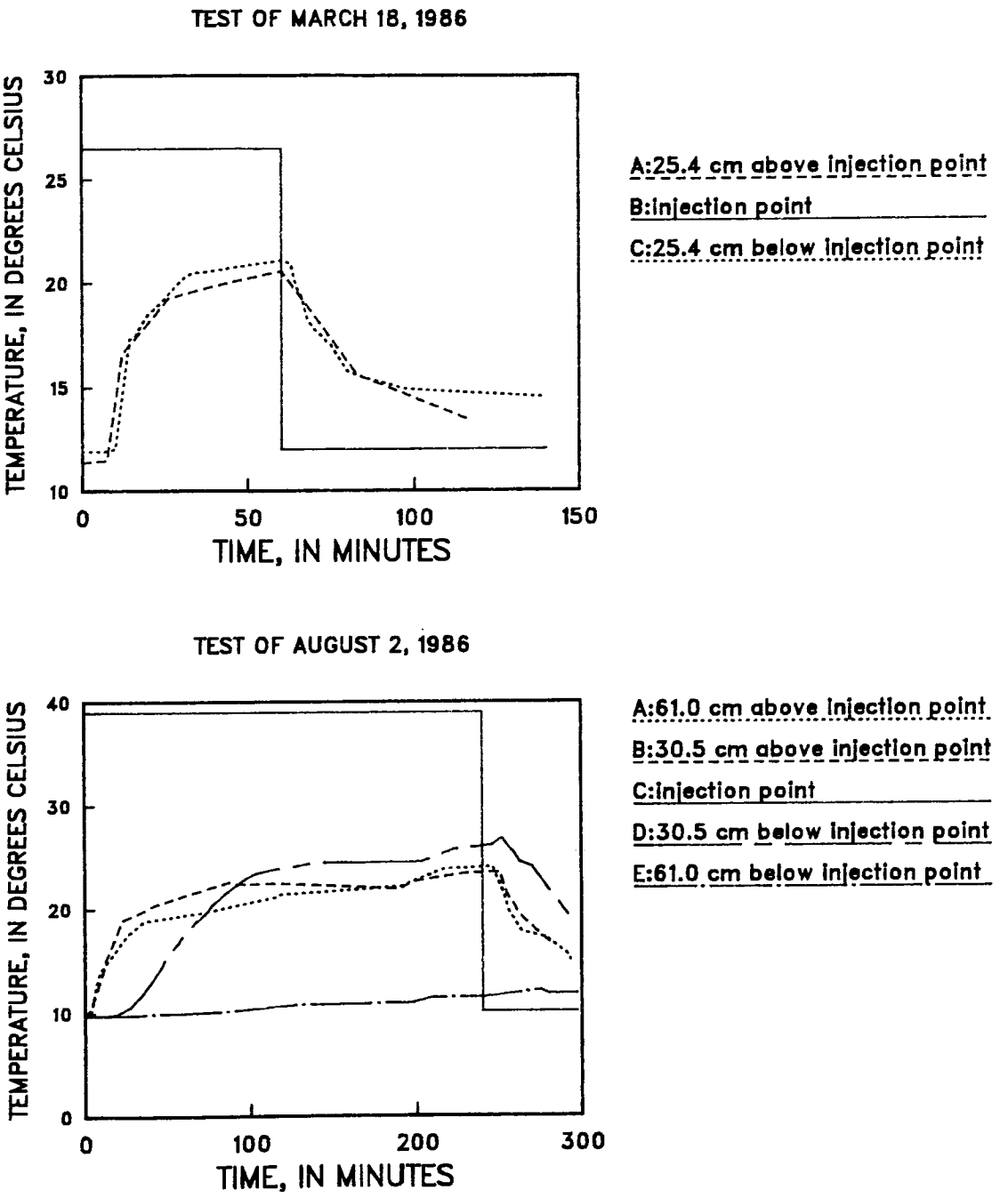

Figure 5.1. Results of small-scale experiments

sion and conduction effects, heat exchange with the solid grains, and interference of the well. This is determined from:

$$V = \frac{4}{3} \pi r^3 \phi_e \qquad (5.1)$$

where V is the volume of water injected, r is the spherical radius, and ϕ_e is the effective porosity (assumed to be 0.38).

A thermal peak of 26.5°C did not occur at either of the observation points because of mixing of the injected plume with ambient ground water by the processes of thermal conduction and dispersion, heat exchange with the solid grains of the aquifer, and, perhaps, some thermal absorption by the sampling well. Assuming a porosity of 0.38, a specific volumetric heat of the solid grains of 1.9×10^6 J/m³°C (de Marsily, 1986), and a specific heat of the water of 4.2×10^6 J/m³°C (de Marsily, 1986), the heat pulse would have lagged behind the water front by a factor of 0.6 (which is 1/1.7, determined from Equations 2.11 and 2.12). Using these estimated values, the peak temperature at the end of the heated-water injection would have occurred at r=23.5 cm (0.6 of 39.1 cm). In addition to the retardation of the thermal plume due to thermal exchange, dispersion about the thermal front also reduced peak temperatures at the observation points.

The results of the August 2 test, in which water at a temperature of 39.0°C was injected at a rate of 1.1 liters per minute, are also shown in Figure 5.1. Although a temperature increase occurred at points 30.5 cm and 61 cm above the injection point (curves A and B), a large increase in temperature did not occur 61 cm below the injection

point (curve E). Also, a much slower rise in temperature is seen at the observation point 30.5 cm below the injection point (curve D).

There are two physical processes which may explain the slow rise in temperature 61 cm below the injection point (curve E). The first process is buoyant flow. Because of the high injection temperature and low injection rate used in this experiment, buoyant forces may have overcome the injection force as the plume moved away from the injection point. The onset of a buoyant plume may have been initiated by an artificially small ratio of horizontal to vertical hydraulic conductivity near the well bore, caused by disturbances to the aquifer during construction of the well. Alternatively, natural heterogeneity of the outwash material may have prevented the injected plume from moving rapidly downward. In either case, the slow rise in temperature 61 cm below the injection point was most likely due to thermal conduction, as opposed to advective thermal transport.

These two small experiments showed that the temperature equipment designed for the thermal experiments would be adequate. The tests also showed the possibility of buoyant flow in the aquifer under unfavorable injection temperatures and injection rates, and served as a qualitative guide in determining the injection temperature used in the 24-hour experiment.

24-hour Thermal Experiment

The temperature of the injected water at the screened interval of the recharge well is shown in Figure 5.2. During the first 45 minutes of the experiment, when the flow field was being developed, the

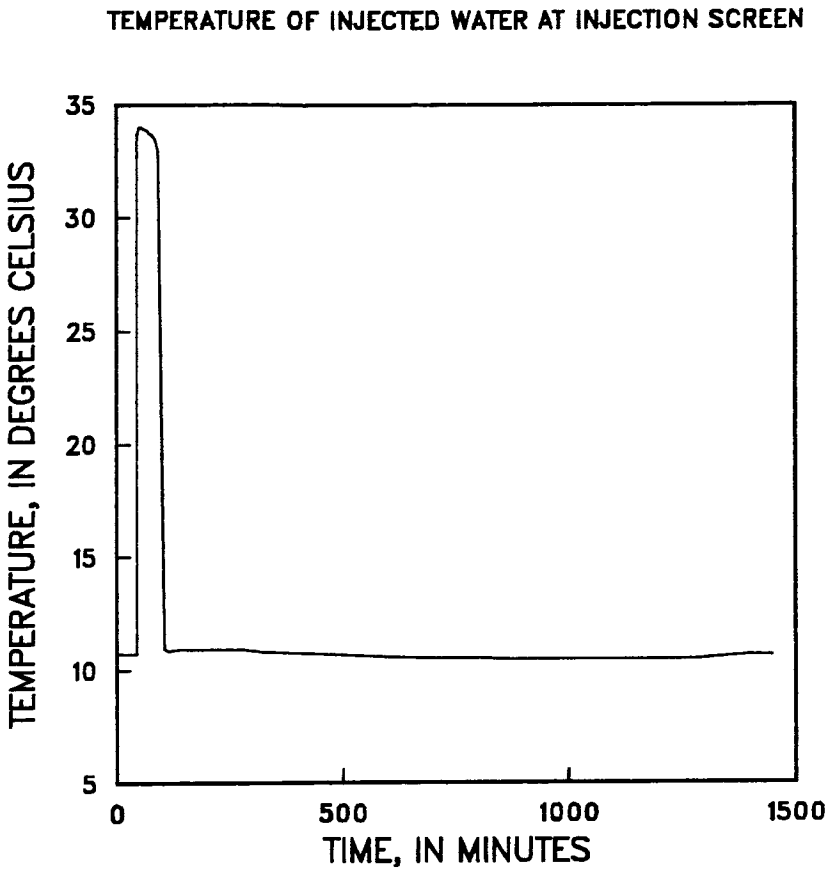

Figure 5.2. Temperature of injected water

average temperature of the injected water was 10.73°C. Temperature of the ground water throughout the aquifer in the area of the injection test prior to the experiment was between 9.65 and 9.76°C. As the water moved through the 3.175-cm transport line, from the supply well to the injection well (approximately 91 m), the temperature of the water rose by 1°C, due to heating in the summer air.

The temperature of the 5.68 m^3 (1,500 gallons) of traced water at the injection screen averaged 33.7°C (a time-weighted average). The temperature of the injected water which followed this hot plume then remained between 10.44 and 10.97°C for the remainder of the experiment. The water cooled progressively through the evening and night to a low of 10.44°C between 12:00 and 7:00 a.m. The temperature of the injected water then rose slowly through the early morning until the test was discontinued at 10:10 a.m.

Temperature and bromide breakthrough occurred at all sampling points (Figures 5.3 and 5.4; Appendix C). The most striking feature of the breakthrough curves is that they indicate that the outwash deposits are vertically heterogeneous. Although the three sampling points at well 5ab span only 0.9 meters (3 feet) vertically, the time to the peak concentration of bromide varies by a factor of approximately 2.6 for the three zones. At well 10dw, the time of arrival of the peak bromide concentration varies by a factor of 2.4 for these three zones (Bb, Y, and G). The heterogeneity of the outwash deposits reflects the dynamically complex geologic environment in which these materials were deposited.

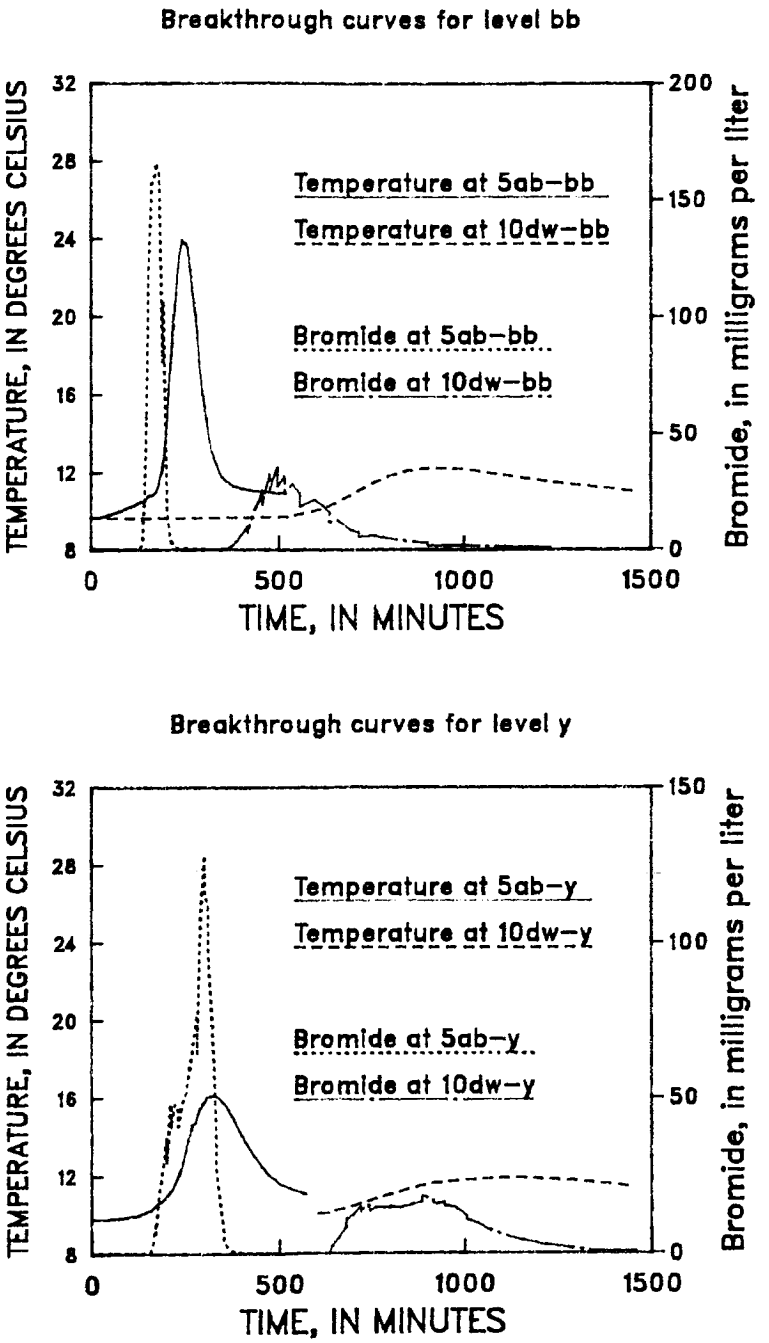

Figure 5.3. Breakthrough curves for levels bb and y

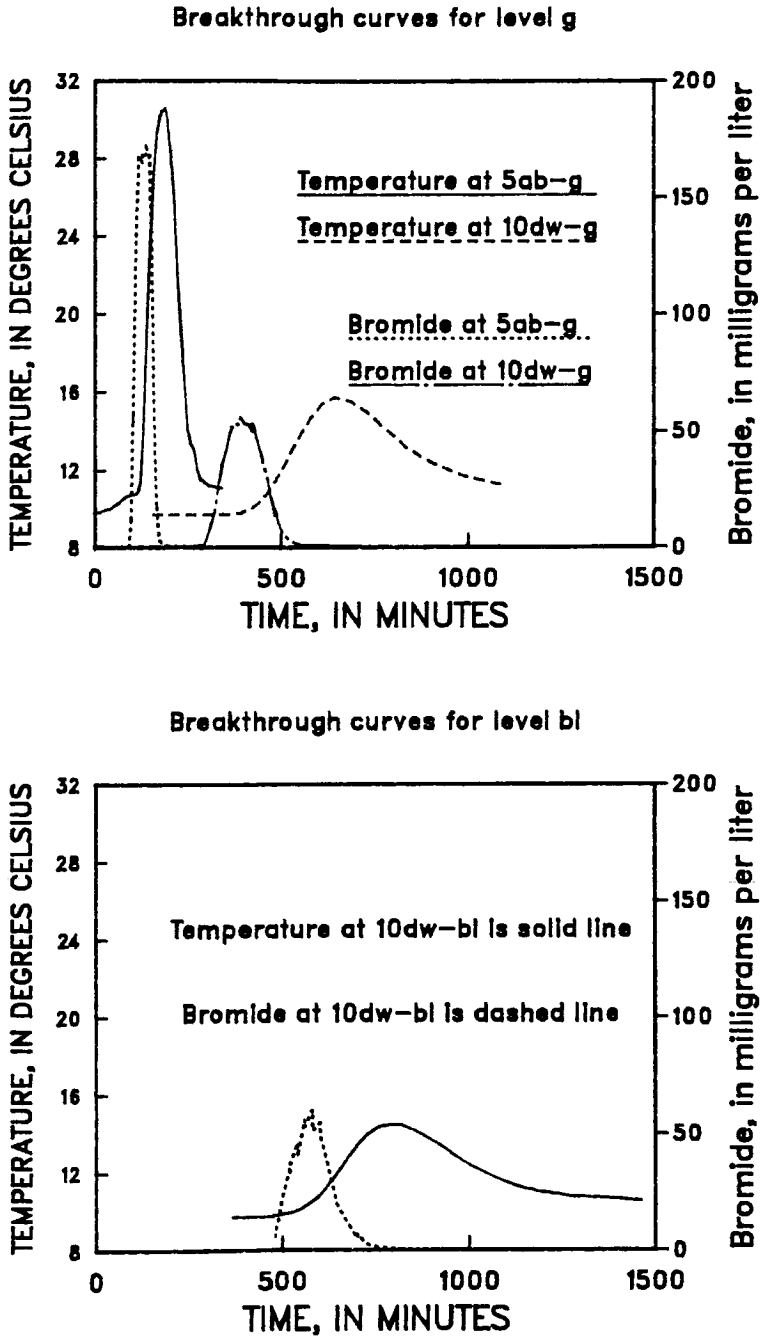

Figure 5.4. Breakthrough curves for levels g and bl

The temperature and bromide breakthrough curves also show the effects of thermal exchange in the porous medium. At each observation point, the peak pore-fluid temperature occurred after the peak bromide concentration. The smallest displacement between the two distributions occurs at points 5ab-y and 10dw-y. This small displacement is likely due to a larger porosity for this zone than for the other zones.

The bromide breakthrough curves for level Y (sampling point 5ab-y and 10dw-y) are characterized by two peaks. The first peak has a steep slope and then levels off (for a short period of time) at about 50 milligrams per liter at point 5ab-y and 15 milligrams per liter at point 10dw-y. This peak is then followed by a second peak, which reaches 128 milligrams per liter at point 5ab-y and 17.5 milligrams per liter at point 10dw-y. Although level Y must consist of material of low permeability, since the elapsed time to the bromide peak for this zone is so long, it is hypothesized that the sampling points also draw water from a thin, more transmissive zone, which contributes to the first peak.

The thermal breakthrough curves at points 5ab-y and 10dw-y do not show this double peak as distinctly as the bromide curves do, although there is a small "bump" in the breakthrough curve at 5ab-y. The reason for the smoother thermal curves is most likely due to the thermal conduction and dispersion processes. As the heat pulse moves slowly through this level of the aquifer, vertical and longitudinal exchange of heat through the stratigraphic layer produces a more even distribution of temperatures. As a result of this spreading of heat, the hypothesized thin zone of higher conductivity at this level becomes

less important to the overall distribution of temperature at the observation points.

The breakthrough curves at observation point 10dw-b1 (Figure 5.4), which is 61 cm below the injection screen, show that the injected water moved vertically as well as radially away from the injection zone. As the thermal energy and chemical mass were spread radially and vertically throughout the aquifer, peak concentrations and temperatures were reduced at points further from the injection well. Since thermal conduction is more important to the vertical exchange of heat than molecular diffusion is to the vertical exchange of mass, there was probably a slightly greater vertical spread in the thermal distribution throughout the aquifer, although there are not enough observation points to verify this.

The arrival of a heat and mass pulse at 10dw-b1 also suggests that forced convection of the injected plume through the aquifer was more important than buoyant forces on the distribution of heat and mass in the aquifer. If the density differences between injected and ambient water had been significant, the arrival of a thermal plume would not have been likely at this observation point (which is located below the injection interval). However, a buoyant flow of heated water over the colder water may have occurred after injection was stopped. Monitoring after the injection pump was turned off would have been necessary to determine if any buoyant instability had been present.

The rise in temperature which occurred at points 5ab-bb, 5ab-y, and 5ab-g during the first 45 minutes of the experiment and shortly after the start of the period of hot water injection (Figures 5.3 and

5.4; Appendix C) indicates that only a small contrast in temperature between injected and ambient waters is needed to produce a measurable change in pore fluid temperature. (During the first 45 minutes of injection, injected water was only 1°C warmer than the ambient water). This is due both to the sensitivity of the instrumentation used and to the high specific volumetric heat capacity of water. The specific volumetric heat of water between 10-30°C is approximately twice the specific volumetric heat of the solid grains, and therefore the water can retain measurable amounts of thermal energy as it moves through the aquifer. This physical characteristic of water is one of the reasons why the use of temperature as a ground-water tracer has been proposed (Davis et al., 1985).

The early periods of the thermal breakthrough curves at these three points show the utility of temperature as a ground-water tracer, when even slight temperature contrasts are used. The contrast in temperature produced at the injected well for the first 45 minutes of the experiment was produced simply by exposing the injected water to the warm summer air and sun. These results suggest that water from a nearby stream, lake, or pond, which differs by only a few degrees from the ground water, could be used as a source of thermal energy (as long as the water was of such chemistry that it would not produce adverse effects on the quality of the ground water). A nearby source of surface water would reduce the need of transporting and containing a large volume of water for injection, which, without the proximity of the Air Base and assistance from the Base personnel, would have been a greater technical problem in this experiment. Chapter Seven will

examine in more detail the minimum injection temperature necessary for detection downstream of a recharge well in an experiment similar to the 24-hour experiment reported here.

CHAPTER SIX

DETERMINATION OF AQUIFER TRANSPORT AND THERMAL PROPERTIES

The preceeding chapter illustrated the usefulness of heated water in delineating hydraulically slow and fast stratigraphic layers of the glacial outwash. It was also shown that buoyant forces did not appear to be significant in the area of the recharge well during the experiment. In this chapter, total porosity and longitudinal thermal and mass dispersivities are determined from the thermal and chemical breakthrough curves. Bulk thermal conductivity and apparent longitudinal thermal dispersivity of the medium are then estimated from the porosity and thermal dispersivity calculations.

Total Porosity

As outlined in Chapter Two, simultaneous measurements of pore-fluid temperature and mass concentration made downgradient of an injection well may be used to estimate aquifer total porosity, if the loss of thermal energy to adjacent stratigraphic layers remains small. If the ratio between the mean arrival time of the thermal plume and the chemical plume at a distance r is designated as "lag", then replacing the velocities of the chemical and thermal fronts by "lag" in Equation 2.11 yields:

$$lag = \frac{\rho_{aq} c_{aq}}{\phi \rho_f c_f} \tag{6.1}$$

or, replacing ρ_{aq} c_{aq} by Equation 2.12:

$$lag = \frac{\phi\rho_f c_f + (1-\phi)\ \rho_s c_s}{\phi\rho_f c_f} \qquad (6.2)$$

Rearrangement of Equation 6.2 leads to an expression for total porosity:

$$\phi = \frac{\rho_s c_s}{(lag-1)\ \rho_f c_f + \rho_s c_s} \qquad (6.3)$$

To determine aquifer total porosity using Equation 6.3, estimates of the densities of the solid and fluid phases, of the specific mass heats of the solid and fluid phases, and of the "lag" term must be made.

The density of water between 10-30°C is 999.7 to 995.7 kg/m^3, while the specific mass heat of water (c_f) in this temperature range is 4191.9 to 4178.2 J/ kg°C (de Marsily, 1986). The specific volumetric heat of water, $\rho_f\ c_f$, is therefore between 4.16 x 10^6 to 4.19 x 10^6 J/ m^3°C. A value of 4.19 x 10^6 J/m^3°C has been used in this analysis.

There is very little variation in the specific mass heats and densities of quartz, plagioclase, and orthoclase minerals (Birch et al., 1942), which comprise 90 to 95 percent of the outwash material near the thermal experiment site. The density of quartz, orthcoclase, and plagioclase feldspars varies between 2.55 to 2.76 gm/cm^3 (Birch et al., 1942; Deer et al., 1966). In this analysis, a solids density of 2.65 gm/cm^3, that of quartz, has been assumed. A specific mass heat of 0.7 J/gm°C, or 700 J/kg°C, has been assumed also, based on the nearly identical values of specific mass heat for quartz, orthoclase, and

plagioclase feldspars (Birch et al., 1942). These estimates of density and specific mass heat yield a specific volumetric heat of the solid grains, $\rho_s c_s$, of 1.86 x 10^6 J/m^3°C. This value is typical of the specific volumetric heat of dry sands (de Marsily, 1986). The assumption that density of the grains is equal to 2.65 gm/cm^3, and that $\rho_f c_f$ is 4.19 x 10^6 J/m^3°C and c_s equals 700 J/kg°C, leads to a maximum error in the porosity determinations made in this analysis of only 2.8 percent, within the range of grain densities of 2.55-2.76 gm/cm^3.

To determine the parameter "lag", which is the ratio of the mean time of arrival of the thermal plume to that of the chemical plume, an estimate of the center of mass of both the chemical and thermal plumes must be made at a sampling point. In this analysis, the first temporal moment was determined for each of the breakthrough curves. The first temporal moment, $\bar{t}$, for either the chemical or thermal breakthrough curve at an observation point, is defined as:

$$\bar{t} = \frac{\sum_{i=1}^{n} t_i Z_i}{\sum_{i=1}^{n} Z_i} \qquad (6.4)$$

where Z_i is either chemical or thermal concentration (above background concentration or temperature) at time t_i, and n is the number of sample points.

The chemical and thermal plume consists of the 5.68 m^3 (1,500 gallons) of tracer solution injected between 45 to 105 minutes, after the flow field was developed. The time at which the first moment

analysis must begin, however, is the time at which hot water began to be injected. Therefore, 45 minutes were subtracted from all sample times, and t = 0 was taken to be the time at which hot-water injection began.

Background concentration of bromide in the aquifer was 0.1 milligrams per liter, both prior to the experiment and during the first 45 minutes of injection. Background temperature of the aquifer was between 9.65 and 9.76°C prior to the experiment at all sampling points. For the periods prior to the hot-water injection and following the hot-water injection, background temperature was increased to approximately 10.7°C at the injection well. This increase in temperature above the initial aquifer temperatures complicated the analysis at sampling points where there was not a very large increase in temperature (i.e., sampling points at well 10dw). At these points, a linear increase in background temperature, from 9.7°C to 10.7°C, was assumed over the period of the experiment. At the observation points at well 5ab, a background temperature of 10.7°C was used. A background temperature of 9.7°C could not have been used at any of the observation points because the trailing edge of the distribution would never have returned to 9.7°C. The difference between using 9.7°C and 10.7°C on the leading edges and during the peak temperatures made little difference in the mean time of arrival at observation points at well 5ab because the bulk of the distributions were concentrated at higher temperatures.

Table 6.1 lists the mean temporal position of the tracers at each of the observation points, determined using the first moment method. Table 6.2 lists the displacement (lag) between the chemical

Table 6.1. Mean temporal position of the thermal and chemical plumes at each of the observation points.

Location	Tracer	Mean Temporal Position[1]
5ab-bb	Bromide	124 minutes
	Heat	204 minutes
5ab-y	Bromide	227 minutes
	Heat	291 minutes
5ab-g	Bromide	87 minutes
	Heat	138 minutes
10dw-bb	Bromide	541 minutes
	Heat	909 minutes
10dw-y	Bromide	820 minutes
	Heat	1093 minutes
10dw-g	Bromide	353 minutes
	Heat	642 minutes
10dw-bl	Bromide	531 minutes
	Heat	773 minutes

1 Mean temporal position is the time after the start of hot-water injection at which the center of mass or heat passes the observation point. Computed from Equation 6.4.

Table 6.2. Displacement of the thermal and chemical fronts (lag) and total porosities determined for each of the observation points.

Location	Displacement (lag)	Total Porosity
5ab-bb	1.65	0.41
5ab-y	1.28	0.61
5ab-g	1.59	0.43
10dw-bb	1.68	0.40
10dw-y	1.33	0.57
10dw-g	1.82	0.35
10dw-bl	1.46	0.49

and thermal plumes and the resulting porosities for each observation point, using Equation 6.3 with $\rho_f c_f = 4.19 \times 10^6$ J/m^3°C and $\rho_s c_s = 1.86 \times 10^6$ J/m^3°C.

The porosities determined for sampling levels BB and G, 0.35-0.43, are in close agreement with the effective porosity of 0.38 determined by LeBlanc et al (in print) using a two-well tracer experiment. The results for level YY, 0.57-0.61, and B1, 0.49, suggest that there are zones of fine sand and silt of high porosity within the outwash material. However, because the bromide breakthrough curves for level Y (Figure 5.3) showed the possibility of extreme variability within this zone, it is possible that these porosity determinations are spurious.

The arithmetic average of aquifer porosity for the seven sampling points is 0.47, which is in good agreement with the results of independent measurements made by LeBlanc and others (in print), who determined an effective porosity of 0.38 for the aquifer. However, there are some inherent limitations to this method of determining aquifer total porosity. First, thermal equilibrium between solid and fluid phases must be attained instantaneously. Second, the porosity determined in this method is termed a total porosity, yet all pores may not contribute to the transport of chemical mass and thermal energy. Non-transporting (dead-end) pores would prevent thermal equilibrium from being attained with portions of the aquifer matrix. The porosity determined under these circumstances would be similar to an effective (or kinematic) porosity. Finally, vertical thermal exchange between each of the sampling levels must be small, to assure that the two

fronts, chemical and thermal, are being transported to each of the sampling points without a proportionally greater loss of thermal energy.

In this experiment, it is possible that thermal equilibrium between solid and fluid phases did not always occur, because of the high ground-water velocities produced near the injection well. The effects of not attaining equilibrium most likely would be an increase in the value of porosity, since there would be less interaction with the solid grains, and heated pore-water would arrive sooner at an observation point.

There is also a possibility that exchanges of thermal energy between stratigraphic layers interferred with the total porosity determinations. The conduction of heat away from the thermal center of mass at a rate greater than the diffusion of chemical mass would increase the volume of material with which the thermal plume is reacting. Therefore, the mean time of arrival of the thermal plume would lag further behind the chemical plume, and a smaller porosity would be determined at an observation point. The results listed in Table 6.2 suggest that this may have occurred in the experiment. A comparison between the porosity values determined at wells 5ab and 10dw for the sampling levels bb, y, and g shows that at each level, the porosity is less further from the injection well. One explanation for this observation is that a portion of the thermal energy was conducted vertically away from each of the the thermal plumes as they were transported through the aquifer, increasing the mean time of arrival to well 10dw and decreasing the total porosity. Alternatively, the decrease in

porosities between the two wells may be due to natural heterogeneity of the aquifer, or analytical and numerical errors in the analysis.

Longitudinal Dispersivity

Longitudinal thermal and mass dispersivities have been determined at six of the sampling points by fitting a theoretical model of longitudinal dispersion in non-uniform flow developed by Gelhar and Collins (1971) to the observed thermal and chemical breakthrough curves. The model of Gelhar and Collins describes the transport of a non-reactive, neutrally buoyant chemical species in a homogeneous, isotropic aquifer under steady flow. The solution considers only longitudinal dispersivity; transverse dispersivity is assumed to be much less than the longitudinal value and is set equal to zero. Their analysis was extended by Voss (1984) for the case of heat transport from an injection well.

There are two main advantages to applying an analytical solution to this problem, as opposed to a computationally more complex numerical model. First, little is known about the hydraulic conductivity of the individual stratigraphic layers at the site, and therefore the use of a numerical code to reproduce the observed data would necessitate approximating hydraulic conductivities throughout the aquifer to best fit the observed data. Second, the analytical solution does not suffer from numerical dispersion or oscillation. These numerical errors become important when the chemical and thermal transport is highly convective, which is assumed to have occurred because of the small scale of the experiment and the steep rising and falling limbs of

many of the breakthrough curves. The main disadvantage to using the analytical model is that a simplified flow field must be assumed near the injection well. In this analysis, radial flow from the injection well is assumed to have occurred.

The equations describing radial transport of mass and heat from an injection well, neglecting the radius of the injection well, are:

For bromide (Gelhar and Collins, 1971; Voss, 1984):

$$C(r,t) = \frac{1}{2}\ (C_{inj}-C_b)\ \mathrm{erfc}\left[\frac{r^2 - r^{*2}}{2\left[\frac{4}{3}\alpha_L r^{*3} + \frac{D_m}{A}\ r^{*4}\right]1/2}\right] + C_b \qquad (6.5)$$

For heat (Voss, 1984):

$$T(r,t) = \frac{1}{2}(T_{inj}-T_b)\mathrm{erfc}\left[\frac{r^2 - r_T^{*2}}{2\left[\frac{4}{3}\beta_L r_T^{*3} + \frac{\lambda_o}{\rho_{aq}c_{aq}}\left(\frac{1}{A_T}\right) r_T^{*4}\right]1/2}\right] + T_b \qquad (6.6)$$

where C_{inj} = injection concentration;

C_b = background concentration;

T_{inj} = injection temperature;

T_b = background temperature;

erfc = complimentary error function;

r = distance from injection screen; and

t = time from start of injection.

[Note: There is a typographical error in Voss (Equation 6.4, 1984). Equation 6.6 is correct (Voss, personal communication, January 8, 1987)].

In the above equations, the velocities of the chemical front, A, and thermal front, A_T, are:

$$A = \frac{Q}{2\pi\phi b}; \qquad A_T = \frac{\phi\rho_f c_f}{\rho_{aq} c_{aq}} \quad A$$

where Q is the injection rate into an aquifer of thickness b. The velocity of the advancing thermal front is displaced behind the chemical front due to thermal interaction with the solid grains, expressed by the factor $\phi\rho_f c_f / \rho_{aq} c_{aq}$.

The positions of the advancing chemical front, r*, and thermal front, r^*_T, are a function of time, and are given by:

$$r^* = (2\ A\ t)^{1/2} \qquad\qquad r^*_T = (2\ A_T\ t)^{1/2}$$

The molecular diffusion coefficient, D_m, has been replaced in Equation 6.6 by the thermal diffusivity of the medium ($\lambda_o / \rho_{aq} c_{aq}$).

To apply Equations 6.5 and 6.6 to the thermal tracer experiment, it is necessary to assume that the plume of injected water moved radially away from the injection well in discrete, homogeneous, and isotropic stratigraphic layers of the aquifer, in which no buoyant flow occurred and in which mass and thermal energy were conserved within each layer. The results of the field experiment suggest that flow may

be viewed as occurring in discrete layers, labeled here as levels BB, Y, and G.

There are, therefore, two unknowns which need to be determined in these equations for each breakthrough curve: the longitudinal dispersivity α_L (or β_L) and the mean velocity of the advancing front A (or A_T). Because there is no indication of how much of the water injected is moving through each layer of the aquifer, it is necessary to make an iterative search for the value of Q_i/b_i (which is incorporated in A_i) which best reproduces the field results at each observation point i.

A FORTRAN computer program was written to determine in an iterative manner the values of α_L (or β_L) and A (or A_t) which best reproduced the observed breakthrough data. A listing of the program is given in Appendix D. A superposition of injection concentrations and temperatures is used. The injection temperatures and concentrations are:

Time (min)	Temperature (°C)	Bromide Concentration (mg/l)
0-45	10.7	0.1
45-105	33.7	173.0
105-end of simulation	10.7	0.1

Background bromide concentration was set equal to 0.1 mg/l, and background temperature was set equal to the temperature of the pore

fluid at each observation point prior to the start of the experiment. The molecular diffusion coefficient was set equal to 6 x 10^{-9} m^2/min and thermal diffusivity ranged from 1.8 to 4.9 x 10^{-5} m^2/min, based on the calculations of bulk thermal conductivity and aquifer specific volumetric heats for each observation point, discussed in the next section. A value of 1.25 x 10^{-7} m^2/min was also used as an upper limit to the molecular diffusion coefficient. The higher value had no effect on the results, however. The range of molecular diffusion coefficients used was based on literature values given by Freeze and Cherry (1979) and de Marsily (1986). The concentrations of bromide against which the analytical solutions were compared were average values of the specific ion electrode and ion chromatographic methods of analysis.

The optimum values of longitudinal dispersivity determined using the analytical, radial flow model are given in Table 6.3. The goodness-of-fit for each of the computed breakthrough curves is given in Figures 6.1-6.6. The best-fit curves were determined by minimizing the sum of the square of the error between observed and computed concentrations or temperatures (see Appendix D) and by visual inspection.

As can be seen in Figures 6.1-6.3, the match between the field breakthrough curves and analytically-derived breakthrough curves at well 5ab is fairly good, except for the bromide curve at observation point 5ab-y. It was not possible to reproduce the double peaks of the bromide curve at observation point 5ab-y (nor at 10dw-y), and the longitudinal mass dispersivities for these two breakthrough curves are essentially meaningless.

Table 6.3. Longitudinal dispersivities determined using the radial flow model.

Location	α_1 (m)	β_1 (m)	β_1/α_1
5ab-bb	.012	.020	1.7
5ab-y	.018	.080	4.4
5ab-g	.014	.016	1.1
10dw-bb	.084	.090	1.1
10dw-y	.100	.124	1.2
10dw-g	.062	.024	0.4

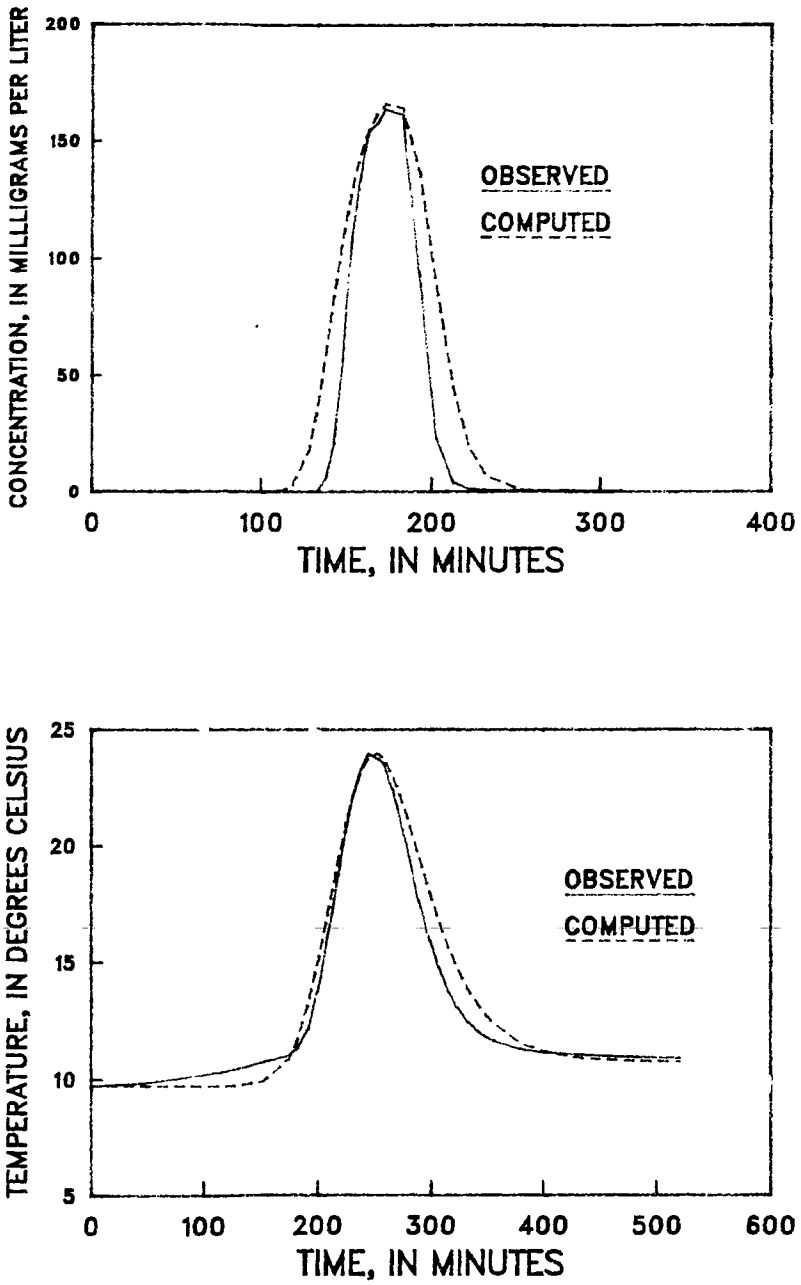

Figure 6.1. Observed and computed distributions at observation point 5ab-bb

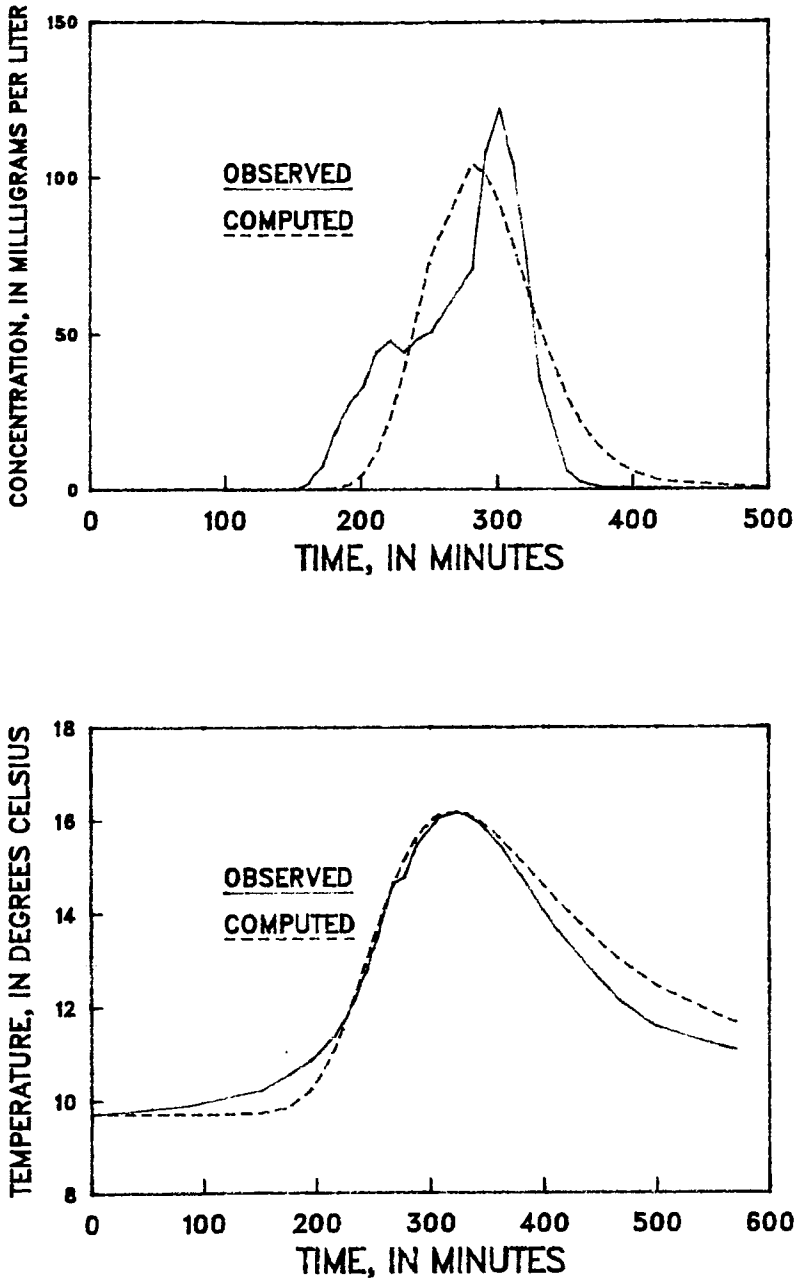

Figure 6.2. Observed and computed distributions at observation point 5ab-y

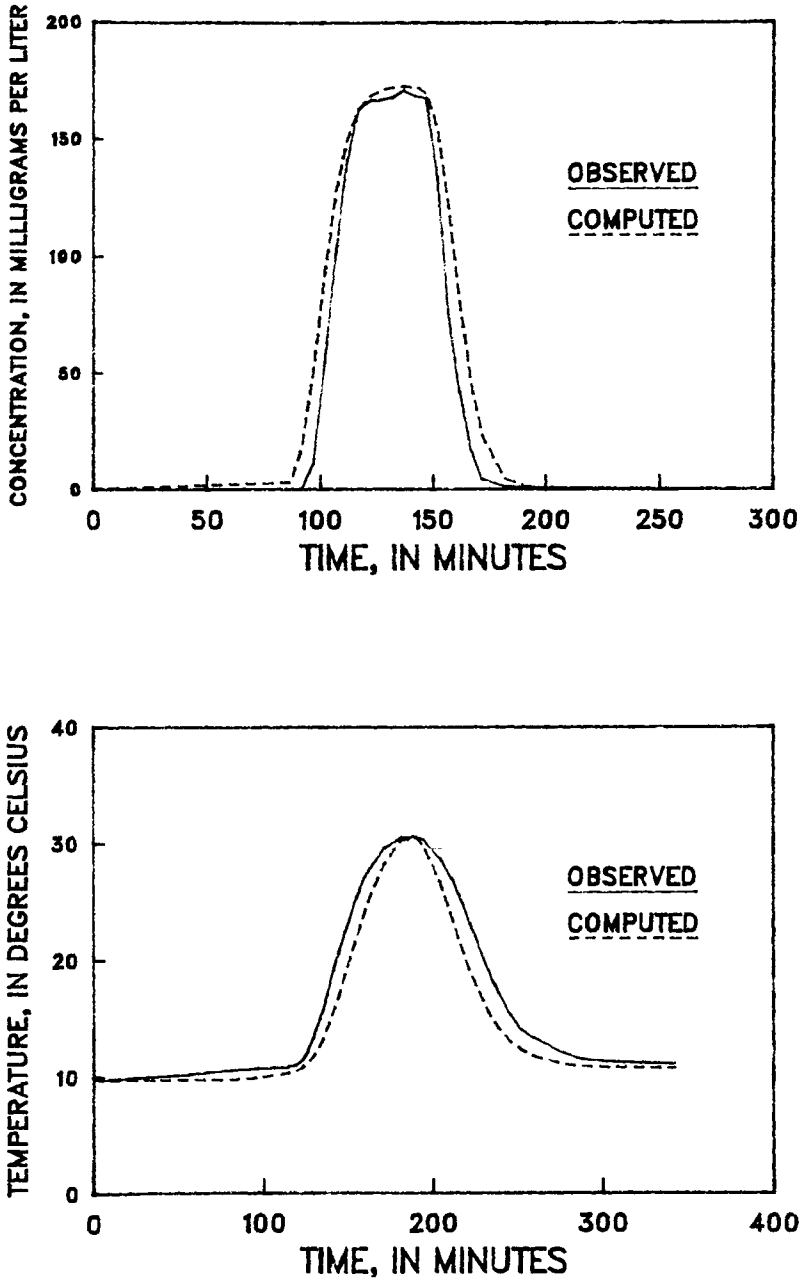

Figure 6.3. Observed and computed distributions at observation point 5ab-g

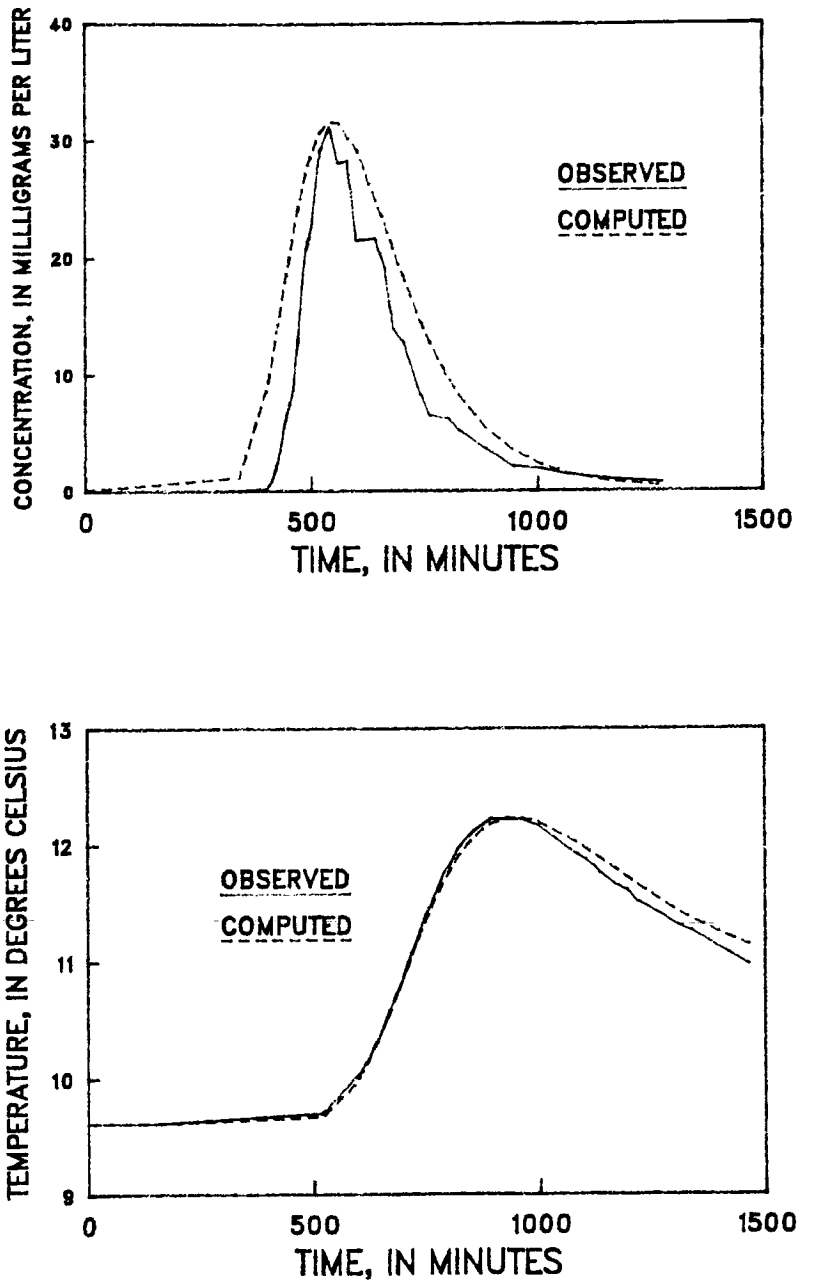

Figure 6.4. Observed and computed distributions at observation point 10dw-bb

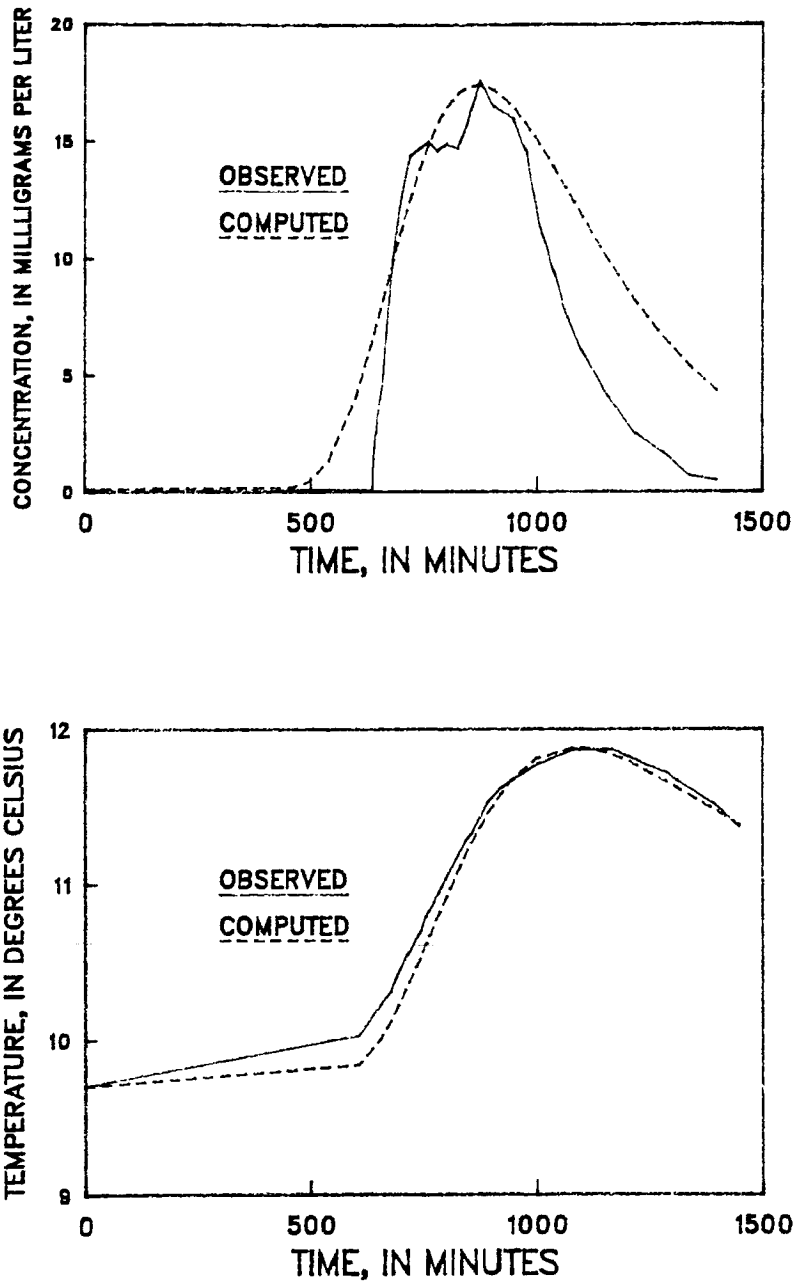

Figure 6.5. Observed and computed distributions at observation point 10dw-y

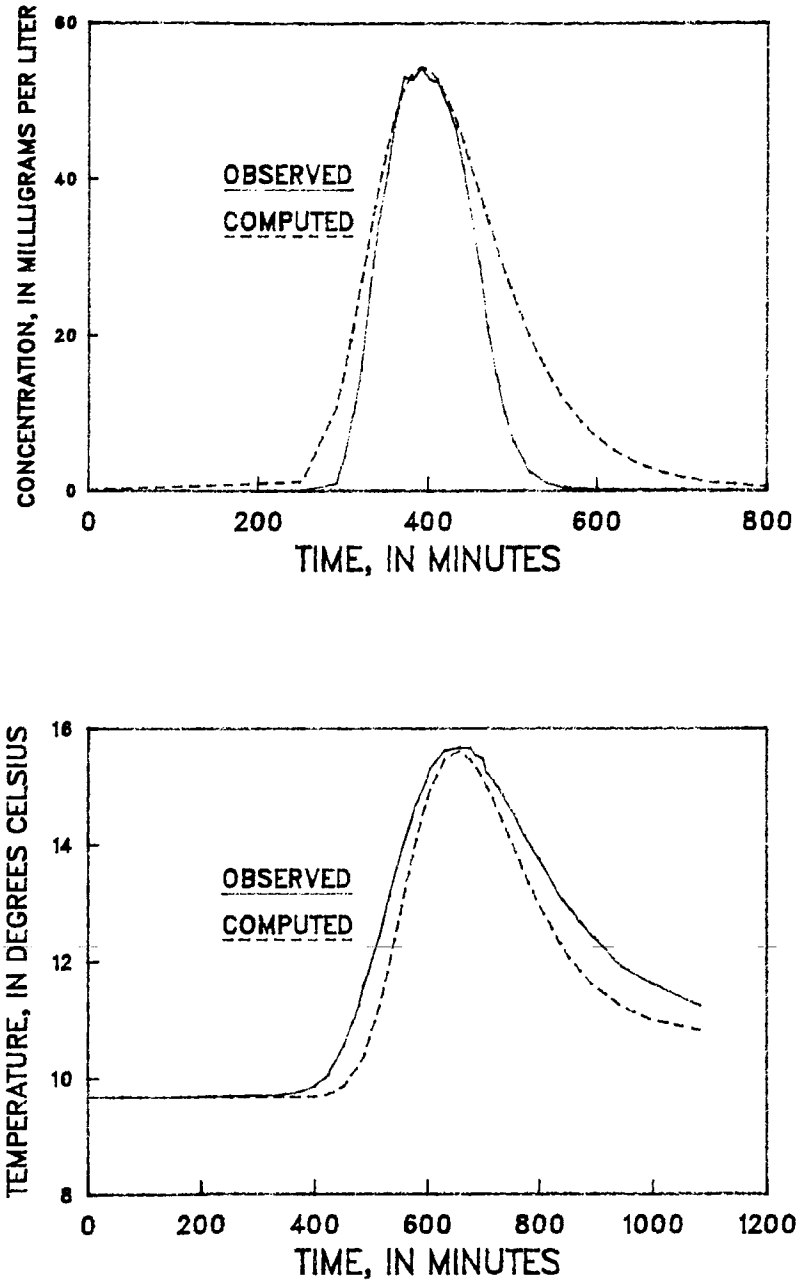

Figure 6.6. Observed and computed distributions at observation point 10dw-g

The results of the analysis for the observation points at well 5ab reinforce the conclusion that buoyant flow was not important to the transport of heat during the experiment. Because the analytical solution does not account for the effects of buoyant forces on heat and mass transport, the match between the theoretical and observed curves would not have been as good if buoyant forces had been important.

Although the match in thermal breakthrough curves at points 10dw-bb and 10dw-y is very good, bromide breakthrough curves at well 10dw (observation points 10dw-bb, 10dw-y, and 10dw-g) and the thermal breakthrough curve at point 10dw-g show the limitations of applying a radial flow model to a system in which the injection screen only partially penetrates the aquifer. The analytically-derived bromide breakthrough curves in Figures 6.4-6.6 (and to a smaller extent the curves for well 5ab) overestimate the total mass passing the observation point. This is because mass and thermal transport is not strictly radial from the injection well, and total mass within a stratigraphic layer is reduced as the plume spreads vertically in the aquifer. Because the vertical spread of the mass and thermal plumes increases as the injected water moves away from the injection well, the most accurate estimates of longitudinal dispersivity are for well 5ab.

The ratio of β_L to α_L (Table 6.3) varies from 0.4 to 1.7, neglecting the results of observation point 5ab-y. These results are consistent with the findings to date on the relative magnitudes of the longitudinal thermal dispersivity and mass dispersivity (de Marsily, 1986; Sauty et al., 1979; Sauty et al., 1982), but do not add to an understanding of the relationship between the asymptotic values of β_L

and α_L. The generally larger values of β_L may be related to a non-equilibrium of thermal energy between solid and fluid phases. Thermal non-equilibrium might cause a greater spread around the mean position of the advancing thermal front, since some energy would be transported with the advancing fluid front while the bulk of the thermal plume reacted with the solid grains. An effective porosity, as opposed to total porosity, would enhance the non-equilibrium between solid and fluid phases, which would then increase the thermal dispersion of the medium.

Bulk and Apparent Thermal Conductivity

Bulk Thermal Conductivity

The bulk thermal conductivity of a porous medium (λ_o) is a function of the volumetric quantities and thermal conductivities of the water and solid phases (Marshall and Holmes, 1979), as well as the packing arrangement and shapes of the solid grains and temperature of the medium (Lunardi, 1981). Bulk thermal conductivity of porous materials may be estimated, however, from empirically-derived and experimentally-determined relationships between bulk density, granular composition and bulk thermal conductivity of a porous medium (Lunardi, 1981).

The porosity of a sediment may be written as (Marshall and Holmes, 1979):

$$\phi = (\rho_s - \rho_b)/\rho_s \qquad (6.7)$$

where ρ_b is the bulk density of the medium (m_s/V_t). Rearrangement of terms in Equation 6.7 yields an expression for bulk density:

$$\rho_b = \rho_s (1 - \phi) \tag{6.8}$$

Because the thermal conductivity of solids is greater than that of water, the thermal conductivity of a medium increases as the porosity decreases and as the bulk density increases (Marshall and Holmes, 1979).

Table 6.4 lists the bulk thermal conductivity for six of the observation points, determined using porosity values given in Table 6.2, a solids density of 2.65 gm/cm^3, and graphical relationships between bulk density and thermal conductivity for coarse-grained materials (Lunardi, 1981).

The bulk thermal conductivities listed in Table 6.4 are slightly lower than those typically listed in the literature for wet sands (Sauty et al, 1979; de Marsily, 1986), but are in good agreement with values cited for coarse-grained aquifers (33 percent porosity) by Parr et al. (1983) and granular, nonconsolidated sandstone (40 percent porosity) by Bear (1972). The very low values for level Y are due to the high porosity of the medium, computed earlier.

Apparent Longitudinal Thermal Conductivity

The estimates of longitudinal thermal dispersivity determined previously may be used to estimate apparent longitudinal thermal conductivities at the observation points. The apparent longitudinal

Table 6.4. Bulk thermal conductivity of the outwash at each sampling point.

Location	Porosity[1]	Bulk Density[2]	Bulk Conductivity[3]
5ab-bb	.41	1.6	2.0
5ab-y	.61	1.0	~1.0
5ab-g	.43	1.5	1.7
10dw-bb	.40	1.6	2.0
10dw-y	.57	1.1	1.1
10dw-g	.35	1.7	2.2

1. From Table 6.2.
2. From Equation 6.8, ρ_s = 2.65 gm/cm^3, in gm/cm^3.
3. From Lunardi (1981, Fig. 4.53) for coarse-grained soils at 4.44°C, in J/sm°C.

thermal conductivity is the effective thermal conductivity of the aquifer during an injection experiment. The apparent longitudinal thermal conductivity is written with respect to the advancing thermal front as (from Equation 2.7):

$$\lambda_L = \lambda_o + \rho_{aq} c_{aq} \beta_L \left| \bar{u}^* \right| \qquad (6.9)$$

The velocity of each of the thermal fronts decreases as the plume moves radially away from the injection well. An average travel velocity may be estimated, however, from the mean time of arrival of the thermal plume at each of the observation points, listed in Table 6.1. These velocities are given in Table 6.6.

The specific volumetric heat of the aquifer, $\rho_{aq} c_{aq}$ at each of the sampling levels is determined using Equation 2.12, with the porosity values determined in the first section of this chapter and density and specific mass heats given previously. Table 6.5 lists the bulk thermal conductivities, porosities, specific volumetric heats, and longitudinal thermal dispersivities used in the estimates of λ_L.

The apparent thermal conductivities and ratios of apparent to bulk thermal conductivities (Table 6.6) are very similar to the results of Sauty et al. (1979) for an alluvial sand and gravel aquifer in Bonnaud, France. Their ranges of λ_L/λ_o are 4-20, and are based on similar injection temperatures and injection rates. The results point to the importance of hydrodynamic thermal dispersion to the overall thermal conductivity of a porous medium during an injection experiment. The apparent thermal conductivities listed in Table 6.6, however, must

Table 6.5. Parameters used in the estimation of apparent longitudinal thermal dispersivity.

Location	Bulk Conductivity	Porosity[2]	$\rho_{aq}c_{aq}$[3]	β_L[4]
5ab-bb	2.0	.41	2.8×10^6	0.020
5ab-y	1.0	.61	3.3×10^6	0.080
5ab-g	1.7	.43	2.9×10^6	0.016
10dw-bb	2.0	.40	2.8×10^6	0.090
10dw-y	1.1	.57	3.2×10^6	0.1
10dw-g	2.2	.35	2.7×10^6	0.024

1. From Table 6.4, J/sm°C.
2. From Table 6.2.
3. Computed using Equation 2.12: $\rho_s c_s = 1.86 \times 10^6$ J/m³°C, and $\rho_f c_f = 4.19 \times 10^6$ J/m³°C.
4. From Table 6.3, m.

Table 6.6. Mean velocity of the thermal fronts, apparent longitudinal conductivity, and ratio of apparent longitudinal conductivity to bulk thermal conductivity.

Location	$\bar{u}$*[1]	Apparent Thermal Conductivity[2]	λ_L/λ_o
5ab-bb	1.4×10^{-4}	9.8	4.9
5ab-y	9.5×10^{-5}	25.9	25.9
5ab-g	2.0×10^{-4}	11.0	6.5
10dw-bb	5.8×10^{-5}	16.4	9.2
10dw-y	4.8×10^{-5}	20.0	18.2
10dw-g	8.2×10^{-5}	7.4	3.4

1. Mean velocity is $r/\bar{t}$, $\bar{t}$ is from Table 6.1, m/s.

2. Computed using Equation 6.9, J/sm°C.

be viewed in light of the many assumptions and limitations involved in the analysis, and reflect any errors made in the computations of the several input parameters (λ_o, β_L, ρ_{aq}, c_{aq}, and $\bar{u}^*$).

CHAPTER SEVEN

SIMULATION OF HEAT TRANSPORT IN A HOMOGENEOUS, ANISOTROPIC AQUIFER

This chapter examines in more detail two conclusions which have been drawn from the field experiments. In Chapter Five, it was noted that measurable changes in pore-fluid temperature had occurred with 1.7 m of the injection well with only a 1°C contrast in temperature between injected and ambient water. The first goal of this chapter is to use a numerical code to simulate the injection of water at 10.7°C into an aquifer at a background temperature of 9.7°C, to determine if significant changes in pore-fluid temperature may be observed at points 1.7 m and 3.1 m downstream of an injection well.

It was also noted in Chapters Five and Six that buoyant flow did not appear to be important to the transport of heat during the thermal experiment. The second goal of this chapter is to simulate the injection of water at a temperature of 33.7°C, and then 65.0°C, into an aquifer with a background temperature of 9.7°C, to determine if buoyant flow under either of these injection temperatures is likely to occur at the injection rate used in the thermal experiment.

The simulations of heat transport in a hypothetical aquifer, hydrogeologically similar to the outwash deposits, have been made with a numerical model of heat transport. The application of a numerical model to heat transport is advantageous because the numerical approximations are well suited to the simulation of density-dependent flow and heat transport in aquifers with complex boundary conditions, which

is not possible with the analytical model used in the preceding chapter. The disadvantages to the use of a numerical code are the computational cost and, as discussed previously, the introduction of numerical errors (dispersion and oscillation).

Model Development

SUTRA, a numerical transport code recently developed by the U.S. Geological Survey was used for the simulations. The model employs a hybrid finite-element and integrated finite-difference approximation to the governing equations of ground-water flow and thermal transport (Voss, 1984). A thorough documentation and listing of the program is given by Voss (1984).

The simulations consisted of a one-hour injection of a thermal plume into a homogeneous, anisotropic aquifer. Injection occurred at the rate of 1.58 liters per second (25.0 gpm) through a 1.2 m (four feet) screened interval of the aquifer, 5.3 to 6.5 m below the simulated top of the aquifer. The plume was preceded for 45 minutes and followed for 1395 minutes by water at a temperature of 9.7°C, which was the background temperature used in all simulations. The total depth of the simulated aquifer was 25.7 m, based on an assumed aquifer thickness of 30.5 m (100 feet), less 4.8 m of unsaturated materials measured prior to the thermal experiment. The thickness of the aquifer was based on an approximate thickness of stratified sand and gravel in the area of the natural-gradient test site (LeBlanc, 1987). Impermeable boundaries were set at the top and bottom of the simulated aquifer and through the radius of the well; therefore, axial-symmetric flow was

assumed (Figure 7.1). A constant-head boundary of 25.7 m was set at a distance of 45 m from the injection well.

The heterogeneity of the aquifer was not considered in the numerical simulations. Instead, a homogeneous, anisotropic aquifer was simulated to obtain a more general result of temperature distributions near the injection well. In actual field experiments, layering of the aquifer will produce contrasts in thermal breakthrough curves similar to the results of the 24-hour thermal experiment. Highly-transmissive zones will result in peak temperatures greater than those predicted in the numerical simulations, while zones of low hydraulic conductivity will reduce peak temperatures.

The transport and thermal input parameters to the numerical model are given in Table 7.1. A horizontal hydraulic conductivity of 0.13 cm (380 feet/day) and an anisotropic ratio of horizontal to vertical hydraulic conductivity of 3.5:1 was used in the simulations, based on the results of LeBlanc et al. (in print). An average value of longitudinal thermal dispersivity of 0.06 m and a porosity of 0.40 were used, based on the analysis of the preceding chapter. Transverse dispersivity was assumed to be 1/100 of the longitudinal dispersivity.

Grid spacings were 0.0625-0.125 m in width near the injection well. The small grid spacing was needed because of the low value of longitudinal thermal dispersivity, and because optimum results are obtained for grid Peclet numbers in the direction of flow, $\Delta X_L/\beta_L$, of between 2 and 4 (Voss, 1984). Grid spacings were increased at distances further from the well where spatial thermal gradients were not as steep. A coarser mesh was initially constructed but was abandoned

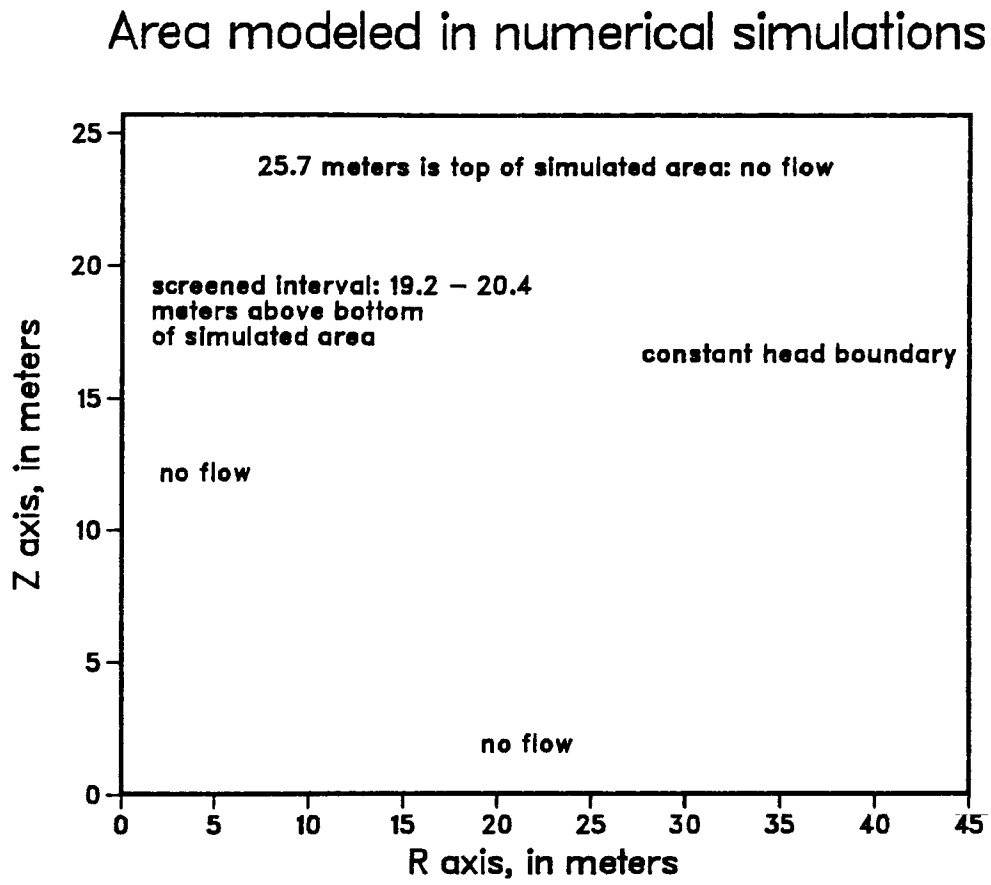

Figure 7.1. Modeled area

Table 7.1. Parameters used in model simulations

Parameter	Value
Horizontal hydraulic conductivity	0.13 cm/s
Vertical hydraulic conductivity	0.04 cm/s
Longitudinal dispersivity	0.06 m
Transverse dispersivity	0.0006 m
Porosity	0.40
Specific mass heat of water	4192 J/kg°C
Specific mass heat of solids	700 J/kg°C
Density of water (at 9.7°C)	999.7 kg/m^3
Density of solids	2650.0 kg/m^3
Thermal conductivity of water	0.6 J/sm°C
Thermal conductivity of solids	3.1 J/sm°C

because of significant numerical oscillations in the breakthrough curves. Time step increments varied between 3 and 24 minutes, increasing in size as the velocity of the front decreased and thermal gradients became less sharp as the plume moved away from the injection well.

Simulation Results

Thermal breakthrough curves at points located 1.7 m and 3.1 m from the injection well at three intervals of the aquifer are shown in Figures 7.2 and 7.3. The points are located at the top, middle, and bottom of the injection screen, 5.3 m, 5.9 m, and 6.5 m below the water table, respectively. The points at the top and bottom of the injection screen were chosen to study the effects of buoyant flow on transport of the thermal plume. A small increase in pore-fluid temperature at points located opposite to the bottom of the injection screen would be indicative of buoyant flow, if the plume had risen above the observation points as it moved through the aquifer.

The similarity between the thermal breakthrough curves at points located at the top and bottom of the injection screen for injection temperatures of 10.7°C and 33.7°C (Figure 7.2) supports the earlier conclusions that buoyant forces were not significant during the 24-hour experiment. The simulated results show that the total thermal mass is nearly identical for the two points at an injection temperature of 33.7°C. A slight variation in the time of arrival and peak temperature for the two points is due to the slightly nonsymmetric distribution of temperatures in the area of the injection well (Figure 7.4). Also, an increase in the hydraulic conductivity of the medium due to

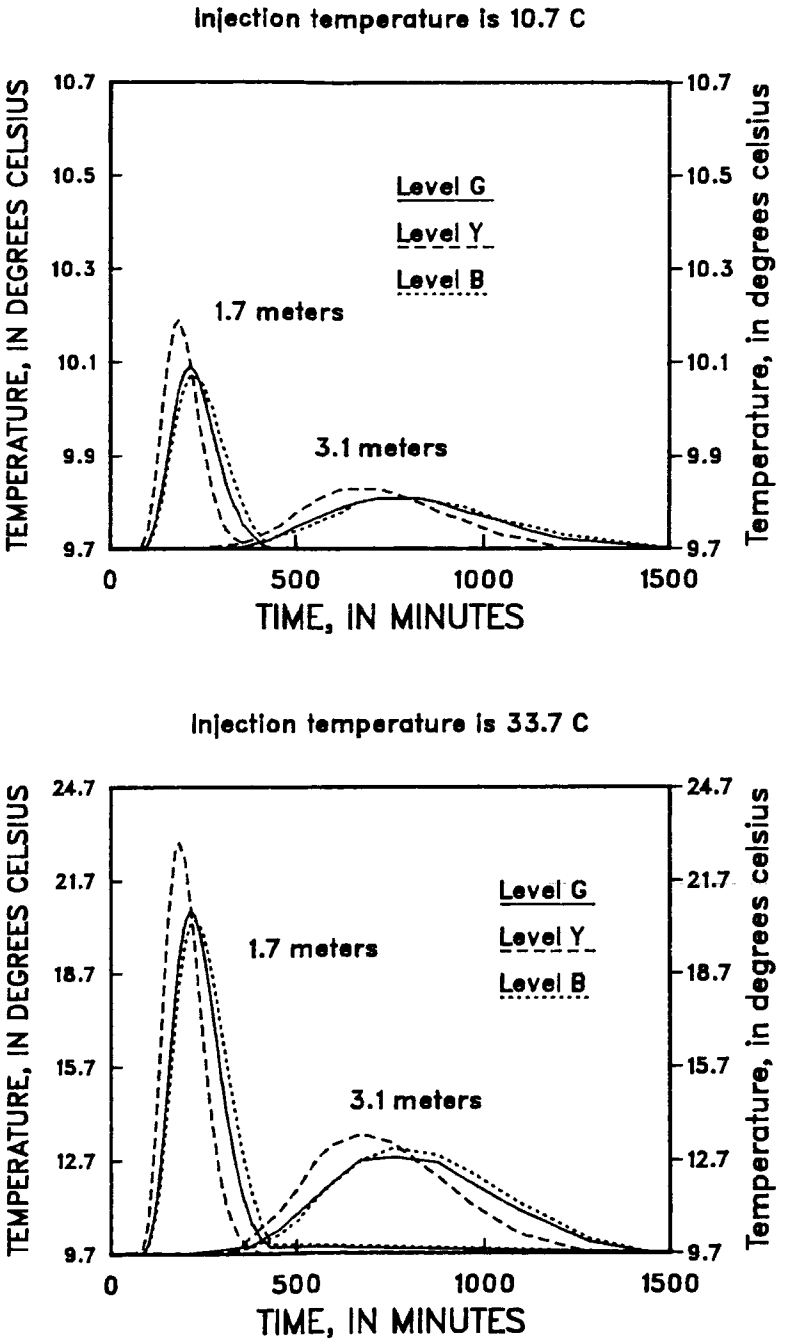

Figure 7.2. Simulation results for injection temperatures of (a) 10.7°C and (b) 33.7°C

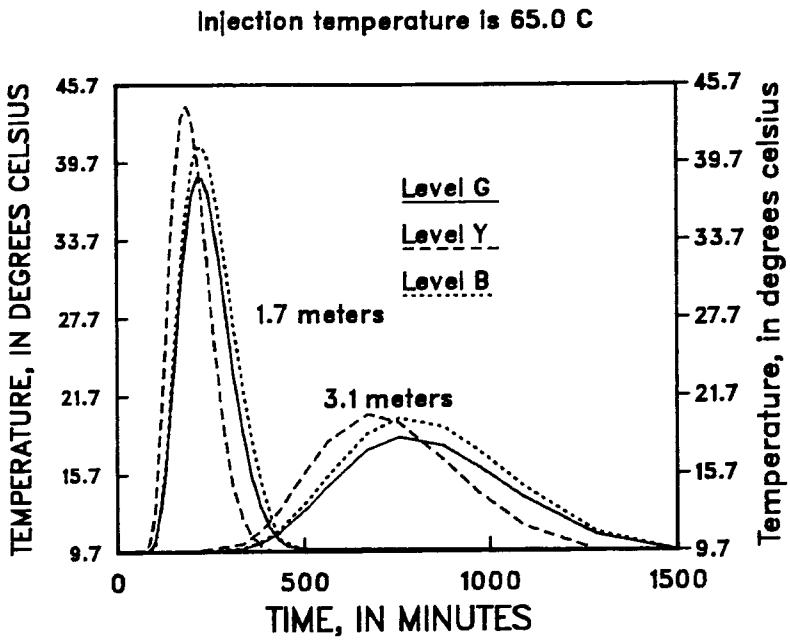

Figure 7.3. Simulation results for injection temperature at 65.0°C

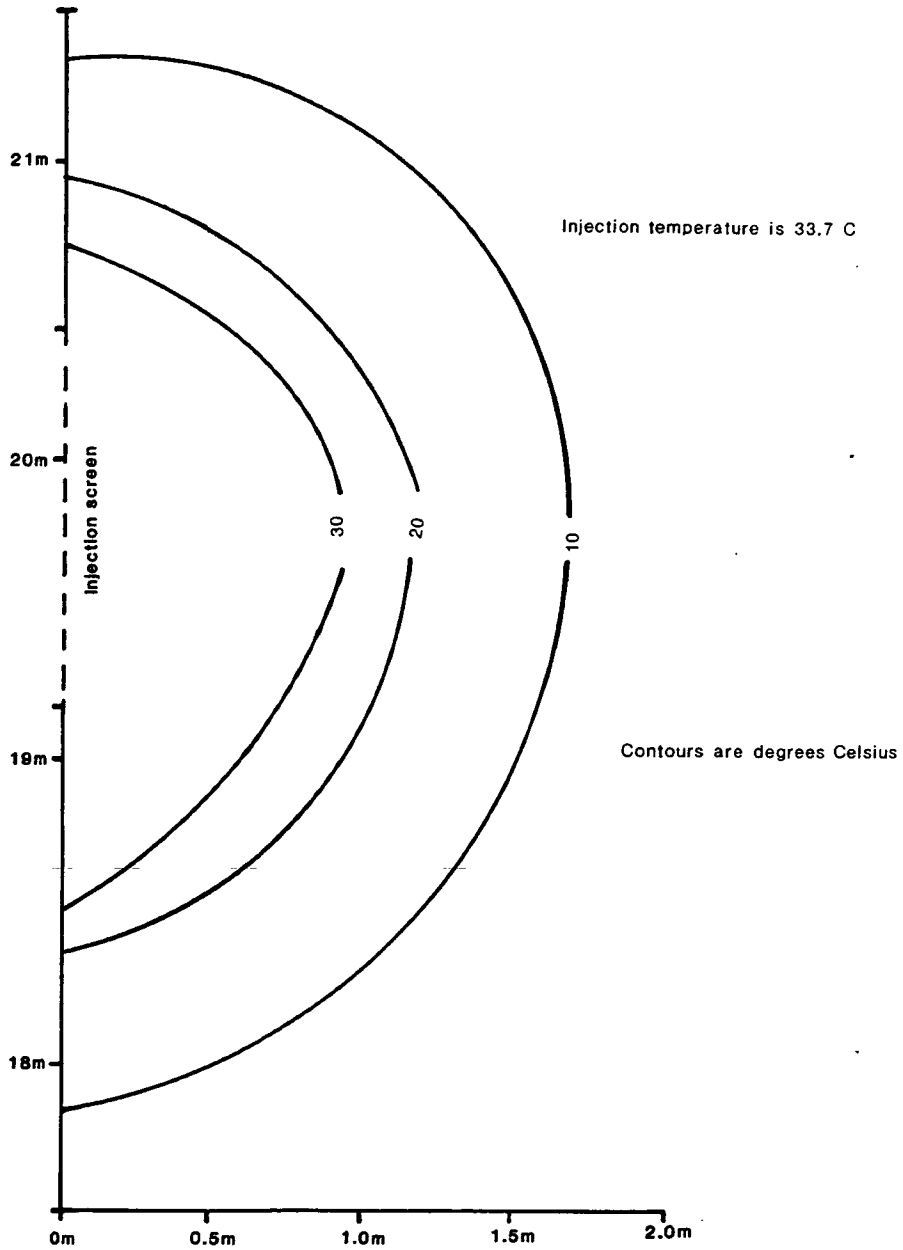

Figure 7.4. Simulation results after 45 minutes of hot-water injection at 33.7°C

the decrease in viscosity at an injection temperature of 33.7°C is not seen to effect the time of arrival nor the time of peak temperature of the distributions, since they are the same for each pair of curves for the two injection temperatures, 10.7°C and 33.7°C.

Figure 7.4 shows a cross-sectional view of the simulated temperature distribution near the injection screen after 45 minutes of injection at 33.7°C. Convective and conductive processes transport the plume both horizontally and vertically, yet there is no indication of a buoyant plume forming on the leading edge of the advancing thermal front.

The breakthrough curves for an injection temperature of 65.0°C (Figure 7.3) begin to show the effect of a buoyant force. The peak temperatures and total thermal mass under the breakthrough curves are greater for the observation point at the top of the injection screen than those at the bottom of the injection screen. The relative contrast between the two points increases at the observation points 3.1 m from the injection well, as the head gradients become increasingly smaller. However, the injection rate is still large enough to overcome vertical buoyant forces, and a breakthrough curve is observed at points opposite the bottom of the injection screen.

Although the results of the simulations are specific to the injection rate used in the 24-hour experiment, they may serve as a qualitative guide in determining the injection temperature used in a ground-water thermal tracer experiment in geologically-similar deposits. The results show that at an injection rate of 1.58 l/s, a large

contrast in injection and ground-water temperatures may be employed in aquifers of small anisotropic ratios.

The simulations have shown also that only a small contrast in temperature between ambient and recharged water is needed to obtain measurable thermal contrasts at points located as far as 3.0 m from the injection screen. Because of the fine sensitivity of the thermal-measuring apparatus, the thermal pulses shown in Figure 7.2a could be monitored accurately at these points. These results are consistent with the field observations discussed in Chapter Five, and reinforce the conclusion that a body of surface water at a slightly different temperature than that of the ground water could be used as a source of injected water.

CHAPTER EIGHT

SUMMARY OF RESULTS AND SUGGESTIONS FOR FURTHER RESEARCH

The results of the thermal experiments have shown that temperature may be used effectively as a ground-water tracer. The thermal breakthrough curves delineated the hydraulically slow and fast layers of the outwash material and could be used to determine aquifer transport and thermal properties, specifically, aquifer porosity, longitudinal thermal dispersivity, and bulk and apparent thermal conductivities. The results of the thermal experiment, as well as the numerical simulations of heat transport, have also shown that small contrasts between injection and ambient waters may be used in a ground-water thermal tracer experiment.

This thesis has outlined the physical processes which affect heat transport in porous materials, and has illustrated how each of these processes affected the results of the thermal tracer experiments. Forced convection produced by the injection of recharge water was the primary mechanisms of heat (and mass) transport in these experiments. The rate at which the injected water was transported through the aquifer during the 24-hour experiment was determined by the permeability of the stratigraphic layer into which the water was injected. As the injected water moved away from the recharge well, thermal dispersion and conduction spread the heat longitudinally and vertically from the center of thermal mass. A comparison to the bromide breakthrough curves has shown that thermal exchange with the solid

grains of the aquifer caused a retardation in the average time of arrival of the thermal plume behind that of the bromide plume. A qualitative analysis of the thermal breakthrough curves and numerical simulations of heat transport in a hypothetical aquifer have shown that buoyant forces and changes to the aquifer's hydraulic conductivity caused by changes in pore-water viscosity were unimportant to the transport of the thermal plume during the 24-hour experiment.

The thermistors used in the temperature-measuring apparatus were reliable and easily adapted to the field conditions. Temperature readings could be made almost continuously, with a very small range of measurement error. One advantage to the use of temperature as a groundwater tracer is that accurate temperature measurements may be made during a field experiment, and there is no need for further laboratory analysis. Preliminary field tests showed that in situ temperature measurements are essential to monitor aquifer thermal conditions accurately.

The greatest technical drawback to the use of temperature as a ground-water tracer in the 24-hour experiment was the large volume of water needed for injection. However, the results of this experiment, as well as subsequent numerical simulations, suggest that surface-water sources may be used in future tracer experiments, which may prove to be less cumbersome.

The analysis of the thermal breakthrough curves has shown that a thermal tracer may be used in conjunction with a conservative chemical tracer to determine aquifer porosity, although the method of analysis will be reliable only under conditions in which two limiting

assumptions are satisfied. These are (1) that thermal equilibrium between solid and fluid phases is attained instantaneously, and (2) that the thermal and chemical plumes are transported to an observation point along the same flow path without a significant loss of thermal energy to adjacent stratigraphic units. As suggested in the following section, further research into the method of analysis should be undertaken to determine other field situations in which the method would be applicable.

The porosities determined in this analysis are comparable to independent porosity measurements of the outwash material, but suggest that local zones of higher porosity may be present; however, the breakthrough curves from which the high porosity values were determined were difficult to analyze and may not be accurate. There are several possible sources of error in the porosity determinations, in addition to the two limiting assumptions discussed above. These include (1) analytical errors in the determination of bromide concentration, (2) numerical errors in the determination of the "lag" parameter, and (3) incorrect assumptions as to the density and specific mass heat of the solid grains.

The small values of longitudinal mass and thermal dispersivities determined from the divergent-flow experiment, 0.012 m-0.124 m, may have resulted from the small scale of the experiment. A comparison with the results of Garabedian et al. (1987), who determined an asymptotic longitudinal dispersivity of 0.96 m for the outwash material, shows that during the divergent-flow, small-scale experiment, longitudinal dispersivities were less than 1/8 to 1/50 of the asymptotic

value determined in the uniform-flow dispersion experiment. The longitudinal dispersivities computed in this thesis differ from the uniform-flow experiment also because the analytical results reflect a match to the observed breakthrough curves for each of the stratigraphic layers and assume no transverse dispersion, whereas the results of Garabedian et al. (1987) are based on a synoptic view of a three-dimensional, multi-stratigraphic plume, in which transverse horizontal and vertical dispersivities are taken into consideration.

Suggestions for Further Research

At least three aspects of this study could be evaluated further by either experimental investigations or analysis of existing data. These are (1) the distance at which a thermal tracer may still be useful at very small temperature contrasts between injected and ambient waters, (2) the application of the methodology for determining aquifer porosity to other field situations, and (3) the determination of the asymptotic relationship between thermal and mass dispersivity at large travel distances of a chemical and thermal plume.

The distance at which an injected plume of water may still yield meaningful results may be studied in either of two ways. First, a field experiment similar to the one reported in this thesis could be conducted with very small temperature contrasts. The test would need to be conducted for a longer length of time if the same injection rate as was used in this experiment was used, but would not necessarily need to include a chemical tracer, which would eliminate the need for sampling and chemical analysis. The use of a conservative chemical

tracer would allow the determination of aquifer porosity, however, and therefore would be a convenient way to further analyze the usefulness and physical soundness of the porosity determination technique.

A second investigation would be to collect available data from an existing thermal plume and determine from the development and movement of the plume the rate of thermal attentuation. This study would necessitate data from a fairly well-monitored plume so that an adequate spatial distribution of temperature in the aquifer at several different times could be determined.

There are at least three field situations in which the methodology to determine aquifer porosity presented in this thesis may be applied. Each of these physical situations is outlined briefly below:

(1) Public supply well which induces infiltration of stream flow. Because stream temperature varies annually, the temperature of water pumped by public supply wells which induce infiltration of nearby streamflow also varies annually. The rate at which the annual temperature variations move through an aquifer is dependent upon the Darcy velocity of the water, the porosity of the aquifer, and the densities and specific heats of the solid and fluid components of the aquifer. If a conservative chemical species could be identified whose concentration in the stream varies in series with the temperature variations of the stream, then monthly measurements of ground-water temperature and concentration of the chemical made at the wellhead should show a

displacement between the time of arrival of the annual pulses of the chemical species and of the heat. This displacement could then be used as the "lag" parameter needed in Equation 6.3 and an average porosity determined for the aquifer between the stream and supply well.

(2) Determination of the mean position of an existing chemical and thermal waste plume. Although the mean temporal positions of the thermal and chemical plumes were used to determine the parameter "lag" in this report, the mean spatial position of each of the plumes at a particular point in time might be used also to determine the displacement between the chemical and thermal pulses. In this example, a wastewater input source with a well-defined conservative plume and a temperature plume would be needed for analysis. The center of mass of the conservative species and the center of thermal mass of the thermal plume could then be compared to determine the "lag" parameter. An average porosity for the aquifer in the area of the plume would then be determined.

(3) Single-well injection/recovery test. A field test could be conducted in which a conservative chemical species and a heat pulse are injected and then recovered by the use of a single well. Measurements of the concentration of the conservative species and of pore-

fluid temperature would be made as the injected plumes are pumped back out of the aquifer. Because the temperature is absorbed by the grains of the aquifer, the time at which the center of the thermal mass is withdrawn at the well will be greater than the time at which the center of the mass of the chemical species is withdrawn, and an average porosity could be determined for the aquifer in the area of the well using Equation 6.3. This idea should be explored further, perhaps with the aid of available numerical or analytical models of heat and mass transport, to identify factors which may complicate the determination of aquifer porosity in a single-well experiment.

To determine the relationship between asymptotic mass and thermal dispersivities, a large-scale dispersion experiment of the type reported by LeBlanc and others (1987) and Garabedian and others (1987) would need to be conducted at a well-monitored field site. The large-scale experiment would necessitate the simultaneous monitoring of chemical and thermal plumes over a period of time long enough for Fickian dispersion to be obtained. Before an experiment of this type is undertaken, however, more research on the thermal attenuation of heat plumes would need to be completed. Because a very small volume of injected tracer is needed (to prevent the uniform flow field from being greatly disturbed during the dispersion experiment), it is possible that a small-volume thermal plume could not be monitored far enough down-gradient of the injection well to yield adequate data. Computer

simulations involving various injection temperatures and volumes as well as various realistic dispersivity values would need to be conducted to determine if such an experiment is feasible.

APPENDIX A

CALIBRATION DATA FOR THERMISTORS

Table A.1. Calibration baths and resistances of thermistors.

	T(°C)	T(°K)	Resistance (ohms) Thermistor 3	4	5	6	7
Bath 1	0.10	273.25	7382	7353	7365	7359	7385
Bath 2	9.89	283.04	4559	4541	4548	4539	4558
Bath 3	35.05	308.20	1483	1479	1481	1479	1484

	T(°C)	T(°K)	Resistance (ohms) Thermistor 1
Bath 1	5.75	278.90	5580
Bath 2	17.97	291.12	3120
Bath 3	28.50	301.65	1950

Table A.2. Coefficients in the Steinhart-Hart Equation.

Thermistor	$\underline{a}$ ($x10^{-3}$)	$\underline{b}$ ($x10^{-4}$)	$\underline{c}$ ($x10^{-7}$)
1	1.52	2.28	1.48
3	1.51	2.29	1.47
4	1.50	2.31	1.40
5	1.50	2.31	1.40
6	1.48	2.35	1.20
7	1.50	2.32	1.34

APPENDIX B

METHOD OF CONSTRUCTION OF WELLS AT THE THERMAL TRACER TEST SITE

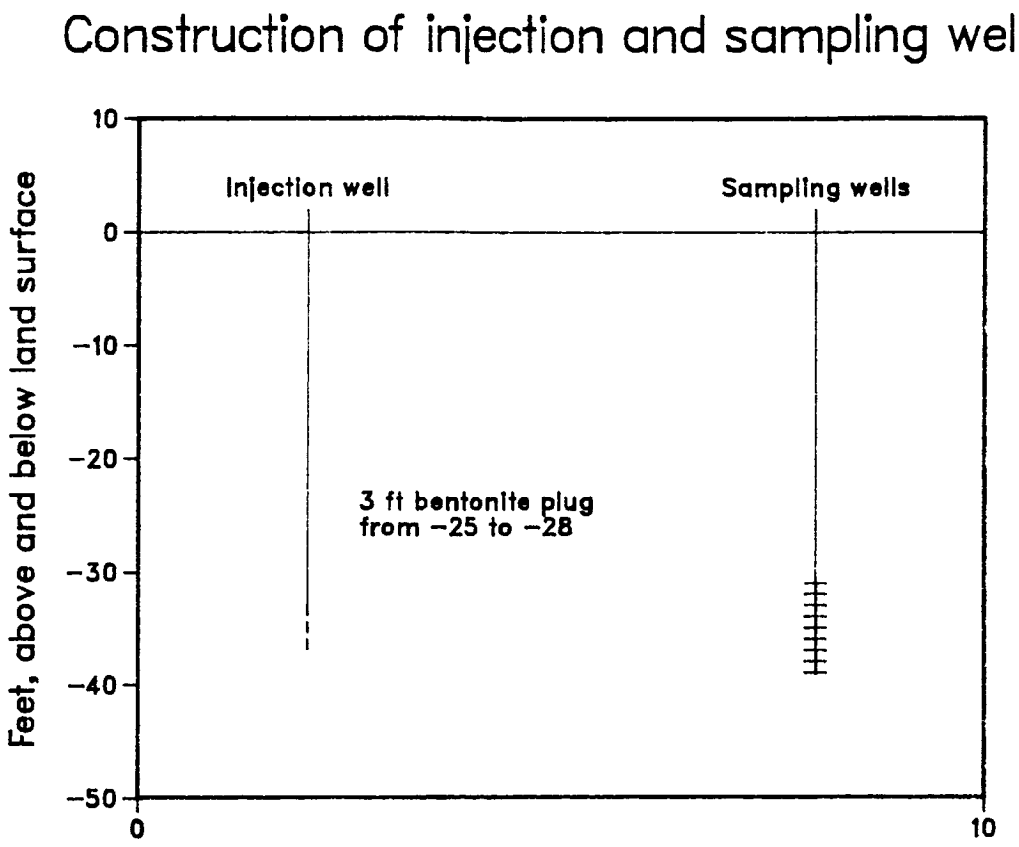

Injection well construction: Schedule 40, 2 inch PVC pipe, screen is 10 slotted PVC. Flush joint, threaded casing. Injection well was augered.

Sampling wells construction: Schedule 40, 1.25 inch PVC pipe, sampling tubes are eighth inch id, quarter inch od polyethylene tubing. nylon mesh stocking over tube hole. Sampling well 5ab has bentonite pellets between sampling points, well 10dw does not. Sampling well 5ab was augered and then washed, 10dw was driven and washed.

Figure B.1. Method of construction of injection and sampling wells

APPENDIX C

DATA FOR THE TWENTY-FOUR HOUR THERMAL EXPERIMENT

Table C.1. Temperature and bromide data for observation point 5ab-bb.

Elapsed Time	Temp (°C)	Elapsed Time	Br (mg/l)	
0	9.70	0	0.1	
24	9.70	48	0.1	
36	9.75	98	0.1	
40	9.75	128	0.1	
48	9.84	133	0.4	
50	9.84	138	4.6	
52	9.84	138	6.7	ic
54	9.84	143	22.1	
55	9.89	143	19.5	ic
57	9.89	148	57.3	
58	9.89	148	56.1	ic
60	9.89	153	100.7	
62	9.89	153	112.7	ic
64	9.93	158	134.2	
66	9.93	163	152.2	
68	9.93	163	157.0	ic
71	9.98	168	157.7	
73	9.98	173	162.1	
76	10.02	173	165.9	
77	10.02	183	161.5	
79	10.02	193	80.5	
80	10.02	193	107.0	ic
84	10.07	203	27.4	
86	10.07	203	18.5	ic
89	10.12	213	4.0	
91	10.12	223	1.1	
94	10.16	233	0.5	
103	10.21	253	0.5	
111	10.30	283	0.2	
115	10.30	313	0.2	
116	10.35			
119	10.35			
121	10.40			
124	10.40			
126	10.40			
128	10.45			
130	10.45			
133	10.49			
136	10.49			
141	10.54			
144	10.59			
153	10.73			
149	10.78			

Table C.1.--Continued

Elapsed Time	Temp (°C)
164	10.83
170	10.93
175	11.02
182	11.31
183	11.42
192	12.13
193	12.39
197	12.92
203	14.33
209	16.09
213	17.08
214	17.35
218	18.69
221	19.51
225	20.60
227	21.09
231	22.11
235	22.73
238	23.27
245	23.93
253	23.74
258	23.55
266	22.46
278	20.20
283	19.13
289	17.69
299	15.97
307	14.80
316	13.70
323	13.09
333	12.44
342	12.03
350	11.77
356	11.62
362	11.52
370	11.42
380	11.27
389	11.22
401	11.12
409	11.12
434	11.02
454	10.97
457	10.97
466	10.97

Table C.1.--Continued

Elapsed Time	Temp (°C)
482	10.93
487	10.93
500	10.88
520	10.88

NOTE: Bromide analyses with an "ic" are results from the ion chromatographic method of analysis. Those with no "ic" have been done with the specific ion electrode.

Table C.2. Temperature and bromide data for observation point 5ab-y.

Elapsed Time	Temp (°C)	Elapsed Time	Br (mg/l)	
0	9.76	0	0.1	
42	9.76	42	0.1	
49	9.81	47	0.1	
51	9.81	72	0.1	
52	9.81	102	0.1	
54	9.81	132	0.1	
55	9.81	147	0.1	
57	9.81	152	0.2	
59	9.81	157	0.7	
69	9.81	162	2.0	
70	9.85	167	4.7	
75	9.85	167	5.6	ic
78	9.85	172	9.1	
80	9.85	172	5.4	ic
88	9.90	182	18.8	
95	9.90	192	27.9	
101	9.94	202	37.3	
112	9.94	202	28.9	ic
113	9.94	212	48.3	
120	9.94	212	40.5	ic
128	10.03	222	47.9	
142	10.13	232	47.6	
146	10.17	232	40.8	ic
152	10.22	242	48.5	
158	10.27	252	50.8	
164	10.36	282	77.1	
166	10.41	282	64.5	ic
170	10.45	292	108.3	
176	10.55	302	128.4	
182	10.64	302	115.1	ic
186	10.69	312	112.6	
194	10.83	312	97.4	ic
197	10.88	322	74.5	
203	11.03	332	41.1	
210	11.22	332	28.0	ic
216	11.37	352	7.7	
220	11.57	352	4.0	ic
224	11.67	362	2.3	
232	12.02	372	1.0	
234	12.17	382	0.4	
244	12.75	392	0.3	
253	13.40	402	0.3	
268	14.65	422	0.2	

Table C.2.--Continued

Elapsed Time	Temp (°C)	Elapsed Time	Br (mg/l)
277	14.76	452	0.2
285	15.24	497	0.2
289	15.49		
297	15.73		
304	15.92		
308	16.05		
314	16.11		
324	16.17		
332	16.11		
341	15.98		
349	15.80		
355	15.67		
363	15.43		
374	15.06		
380	14.82		
388	14.53		
400	14.07		
409	13.73		
413	13.62		
433	13.02		
453	12.49		
465	12.17		
470	12.07		
483	11.87		
500	11.57		
529	11.32		
560	11.12		
565	11.07		
570	11.07		

Table C.3. Temperature and bromide data for observation point 5ab-g.

Elapsed Time	Temp (°C)	Elapsed Time	Br (mg/l)	
0	9.80	0	0.1	
15	9.84	47	0.1	
28	9.97	52	0.1	
41	10.02	57	0.1	
48	10.11	67	0.1	
49	10.11	77	0.1	
51	10.16	87	0.1	
53	10.16	92	0.6	
54	10.20	97	11.8	
56	10.20	97	10.6	ic
58	10.25	102	57.0	
59	10.25	102	52.3	ic
60	10.25	107	101.3	
61	10.30	107	101.2	ic
63	10.30	112	141.1	
65	10.34	117	157.9	
67	10.39	117	167.6	ic
70	10.44	122	166.6	
72	10.44	127	164.7	
74	10.49	127	169.2	ic
77	10.53	132	167.9	
78	10.53	137	168.6	
79	10.53	137	173.2	ic
80	10.58	142	168.6	
83	10.58	147	166.6	
85	10.63	147	168.5	ic
86	10.63	152	134.2	
88	10.68	157	80.3	
92	10.68	157	70.9	ic
96	10.72	162	42.0	
98	10.77	167	16.1	
102	10.77	167	16.9	ic
107	10.77	172	5.3	
110	10.77	172	3.2	ic
114	10.82	182	1.2	
115	10.87	192	0.6	
118	10.92	202	0.5	
118.5	10.96	212	0.3	
119	11.01	222	0.3	
120	11.06	232	0.2	
121	11.16	242	0.2	
122	11.31			
123	11.41			

Table C.3.--Continued

Elapsed Time	Temp (°C)	Elapsed Time	Br (mg/l)
123.5	11.51		
124	11.56	292	0.2
124.8	11.76		
125	11.86		
126	12.17		
126.5	12.27		
127	12.48		
129	13.18		
132	14.19		
133	14.89		
134	15.25		
135	15.68		
137	17.03		
139	17.78		
141	19.07		
143	20.06		
144	20.54		
147	22.03		
148	22.38		
149	23.09		
151	23.74		
152	24.31		
155	25.40		
158	26.55		
159	26.99		
160	27.21		
161	27.43		
163	27.89		
165	28.35		
167	28.83		
171	29.57		
177	30.20		
179	30.33		
181	30.46		
190	30.59		
191	30.46		
194	30.33		
197	29.94		
204	28.71		
211	26.99		
215	25.70		
219	24.11		
222	23.09		
225	21.86		

Table C.3.--Continued

Elapsed Time	Temp (°C)
233	19.07
236	18.06
239	17.17
243	16.12
246	15.31
252	14.01
259	13.34
267	13.07
277	12.01
284	11.61
288	11.46
298	11.31
303	11.26
309	11.16
313	11.16
325	11.11
334	11.06
342	11.06

Table C.4. Temperature and bromide data for observation point 10dw-bb.

Elapsed Time	Temp (°C)	Elapsed Time	Br (mg/l)	
151	9.61	342	0.1	
196	9.61	392	0.1	
248	9.61	402	0.3	
288	9.61	412	0.8	
328	9.61	422	1.8	
368	9.61	432	3.4	
395	9.61	442	5.4	
499	9.70	442	5.9	ic
521	9.70	452	7.4	
530	9.74	462	9.9	
565	9.88	462	7.5	ic
580	9.93	472	12.7	
585	9.97	482	17.6	
595	10.01	492	20.8	
615	10.11	502	25.7	
622	10.16	502	19.3	ic
632	10.25	522	33.3	
641	10.30	522	25.1	ic
655	10.44	542	35.4	
667	10.58	542	27.0	ic
669	10.68	562	31.5	
689	10.77	562	24.7	ic
699	10.87	582	28.3	
707	10.97	602	24.4	
716	11.07	602	18.5	ic
727	11.16	642	21.7	
744	11.36	662	19.3	
755	11.46	682	16.1	
774	11.61	682	11.8	ic
789	11.76	702	12.9	
799	11.81	742	8.3	
821	11.97	762	7.4	
842	12.07	762	5.6	ic
855	12.12	802	6.2	
874	12.17	827	5.2	
892	12.22	887	3.6	
921	12.22	947	2.5	
929	12.22	947	1.6	ic
944	12.22	1007	1.9	
954	12.22	1067	1.4	
960	12.22	1157	1.0	
995	12.17	1277	0.7	
1082	11.92			

Table C.4.--Continued

Elapsed Time	Temp (°C)
1103	11.87
1123	11.81
1135	11.76
1149	11.71
1168	11.66
1194	11.61
1202	11.56
1219	11.51
1240	11.46
1266	11.41
1284	11.36
1306	11.31
1333	11.31
1338	11.26
1389	11.16
1419	11.07
1449	11.02
1464	10.97

Table C.5. Temperature and bromide data for observation point 10dw-y.

Elapsed Time	Temp (°C)	Elapsed Time	Br (mg/l)	
608	10.03	637	0.2	
632	10.08	642	2.0	
643	10.17	662	5.1	
654	10.22	682	8.5	
667	10.27	682	11.1	ic
678	10.31	702	12.6	
688	10.41	722	15.2	
698	10.45	722	13.6	ic
708	10.50	742	16.0	
716	10.55	742	13.3	ic
727	10.64	762	15.0	
743	10.69	782	14.6	
756	10.79	802	14.5	
773	10.88	802	15.2	ic
790	10.98	827	14.7	
799	11.03	857	15.7	
820	11.12	887	16.7	
842	11.27	887	18.4	ic
855	11.32	917	17.5	
873	11.42	917	15.4	ic
892	11.52	947	16.6	
900	11.57	947	15.4	ic
921	11.62	977	14.6	
945	11.67	1007	11.9	
999	11.77	1007	10.8	
1081	11.87	1037	9.5	
1104	11.87	1067	7.4	
1122	11.87	1067	7.6	
1135	11.87	1097	6.1	
1149	11.87	1157	4.0	
1167	11.87	1157	4.2	ic
1194	11.82	1217	2.5	
1203	11.82	1277	1.7	
1218	11.77	1337	0.7	
1239	11.77	1397	0.5	
1267	11.72	1457	0.7	
1284	11.72			
1307	11.67			
1335	11.62			
1390	11.52			
1420	11.47			
1447	11.37			
1462	11.37			

Table C.6. Temperature and bromide data for observation point 10dw-g.

Elapsed Time	Temp (°C)	Elapsed Time	Br (mg/l)	
156	9.67	222	0.1	
195	9.67	252	0.1	
248	9.67	292	1.1	
287	9.67	292	0.8	ic
328	9.71	302	4.4	
345	9.71	312	9.7	
364	9.71	322	16.1	
368	9.71	322	15.4	ic
375	9.76	332	25.5	
397	9.80	342	34.3	
399	9.85	342	35.1	ic
418	9.99	352	40.9	
423	10.03	362	48.3	
428	10.13	372	53.1	
443	10.36	372	53.3	ic
452	10.55	382	52.9	
479	11.23	392	52.9	
487	11.58	392	55.8	ic
497	11.83	402	52.9	
514	12.40	412	52.5	
520	12.61	422	49.9	
532	13.10	422	52.8	ic
538	13.32	432	47.0	
546	13.60	442	41.7	
558	13.99	442	42.0	ic
567	14.28	462	29.5	
580	14.69	462	29.2	ic
586	14.81	472	21.2	
595	14.99	482	13.6	
605	15.30	482	16.3	ic
614	15.48	492	10.2	
631	15.61	502	6.4	
640	15.73	502	6.5	ic
656	15.67	522	2.5	
666	15.67	542	1.1	
678	15.54	562	0.5	
689	15.48	582	0.3	
698	15.36	602	0.2	
707	15.24	622	0.2	
716	15.11	702	0.1	
726	14.99			
745	14.69			
751	14.58			

Table C.6.--Continued

Elapsed Time	Temp (°C)
756	14.46
772	14.17
790	13.88
798	13.77
820	13.38
841	13.05
856	12.88
872	12.67
893	12.46
897	12.40
921	12.20
946	11.99
952	11.94
995	11.63
1083	11.23

Table C.7. Temperature and bromide data for observation point 10dw-b1.

Elapsed Time	Temp (°C)	Elapsed Time	Br (mg/l)	
367	9.70	481	5.6	
395	9.70	481	7.9	
426	9.70	491	13.6	
476	9.74	491	14.6	
477	9.79	501	22.9	
497	9.84	521	35.0	
521	9.93	521	32.9	ic
531	9.97	521	36.8	ic
549	10.11	541	46.3	
558	10.20	541	39.9	ic
568	10.34	561	55.9	
581	10.53	561	52.4	ic
585	10.58	581	60.2	
595	10.72	581	50.9	ic
615	11.16	601	54.6	
633	11.61	601	49.2	ic
641	11.81	621	36.8	
655	12.17	641	23.5	
667	12.53	641	21.1	ic
679	12.85	661	15.0	
688	13.07	701	4.9	
699	13.34	701	6.9	ic
708	13.56	721	2.7	
717	13.77	741	1.6	
726	13.96	761	1.1	
744	14.19	801	0.4	
757	14.36	826	0.2	
772	14.42	856	0.2	
791	14.48			
798	14.48			
819	14.42			
841	14.24			
856	14.13			
874	13.96			
892	13.73			
922	13.40			
947	13.07			
952	12.96			
999	12.38			
1081	11.61			
1205	11.46			
1123	11.31			
1134	11.26			

Table C.7.--Continued

Elapsed Time	Temp (°C)
1150	11.16
1167	11.11
1195	10.96
1203	10.96
1219	10.92
1227	10.87
1240	10.87
1267	10.77
1284	10.72
1307	10.72
1336	10.68
1390	10.63
1421	10.58
1448	10.53
1463	10.53

Table C.8. Temperature of injected water at injection well.

Elapsed Time	Temp (°C)
0	9.70
1	10.73
10	10.73
43	10.73
46	10.73
46.3	10.78
47.3	32.94
47.7	33.69
52	33.99
53	34.15
57	33.99
61	33.99
70	33.84
77	33.69
85.5	33.53
89.3	33.38
95.3	32.94
107.7	10.92
117.3	10.83
127.7	10.83
144	10.92
157	10.78
165	10.97
212	10.92
237	10.92
278	10.92
295	10.83
325	10.78
372	10.73
414	10.68
455	10.68
496	10.63
522	10.63
560	10.59
600	10.54
624	10.54
680	10.49
728	10.49
749	10.49
800	10.49
857	10.44
908	10.44
991	10.44
1083	10.44

Table C.8.--Continued

Elapsed Time	Temperature (°C)
1151	10.44
1195	10.44
1225	10.44
1241	10.44
1268	10.44
1285	10.49
1306	10.54
1332	10.59
1392	10.68
1421	10.73
1449	10.63

APPENDIX D

COMPUTER PROGRAM TO COMPUTE LONGITUDINAL DISPERSIVITY

```
      program disp
c     Program to estimate longitudinal dispersivity using a
c      radial flow model. Based on an analysis by Gelhar and
c      Collins (1971) and extended by Voss (1984).
c
c     Paul Barlow, May 20, 1987

      real t(27),c(27),c0,c1,r,a,diff,alpha,alpha2,alphamax,
     /sumerr,minerr,c2
      integer n,i,j
      open(unit=1,file='disp.out',status='new')

c     Fill t and c matrices. These are sampling times and
c      concentrations (or temperatures) against which the
c      analytical solution will be compared in the least
c      squares minimization section.
c     This example is for observation point 10dw-g, bromide
      data t/0,252,292,302,312,322,332,342,352,362,372,382,392,
     /402,412,432,442,462,472,482,492,502,522,542,562,582,602/
      data c/.1,.1,1.,4.3,9.6,15.5,25.4,34.6,40.8,48.2,53.1,
     /52.8,54.3,52.8,52.4,46.9,41.7,29.3,21.1,14.9,10.1,6.4,2.4,
     /1.,0.4,0.2,0.1/
      write(1,1)
  1   format('  ouput for 10dw-g, bromide')

c  n = number of sample points; r = radial distance from injection
c    well; c0 = background concentration (or temperature);
c    c1 = first (and third) injection concentration; c2 = second
c    injection concentration; diff = chemical molecular diffusion
c    coefficient (or thermal diffusivity)
      n=27
      r=3.14
      c0=0.1
      c1=0.1
      c2=173.
      diff=0.000000006

C   Find the optimum velocity (a) and longitudinal dispersivity
c    (alpha):
      minerr=10000000
      do 20 k=10,30
       a=.0005*k
      do 5 i=10,35
       alpha=.002*i
       sumerr=0.0
       do 10 j=1,n
       time=t(j)
       call concen(time,cest,alpha,a,diff,r,c0,c1,c2)
c   Minimize the sum of the error
       sumerr=sumerr + (cest-c(j))**2.0
  10   continue
```

```
      if(sumerr.lt.minerr)then
       minerr=sumerr
       alphamax=alpha
       amax=a
      endif
    5 continue
   20 continue

      write(1,2)minerr,alphamax,amax
    2 format(/,'  minimum sum of error is  ',f10.2,/,'  optimum
     / longitudinal dispersivity is  ',f5.3,/,'  optimum a is ',
     /f6.4,/)
      write(1,3)
    3 format('  time      observed concen.    estimated concen.')

c  Write optimum match to output file: alphamax is optimum
c   dispersivity, amax is optimum velocity, minerr is the
c   minimum sum of the error between the observed and computed
c   concentrations (or temperatures):
      do 15 i=1,n
       time=t(i)
       call concen(time,cest,alphamax,amax,diff,r,c0,c1,c2)
       write(1,4)time,c(i),cest
    4  format(2x,f6.1,8x,f6.2,19x,f6.2)
   15 continue

      close(unit=1)
      stop
      end

c  Subroutine to compute analytical concentration (or
c    temperature) using a superposition of injection
c    concentrations (or temperatures) in the 24-hour
c    thermal experiment. This subroutine is based on
c    equations given in Chapter 6 of the thesis, under
c    'longitudinal dispersivity'.
c    The equations are based on Gelhar and Collins (1971)
c    and Voss (1984).
      subroutine concen(time,cest,alpha,a,diff,r,c0,c1,c2)
      diff2=diff/a
      alpha2=1.33333*alpha
      if(time.le.45)then
       rstar=2*a*time
       top=r**2-rstar
       bota=alpha2*(rstar**1.5)
       botb=diff2*(rstar**2.0)
       bot=2*sqrt(bota+botb)
       if(bot.eq.0.0)bot=.000000001
       x=top/bot
       cest=.5*(c1-c0)*erfc(x) + c0
      endif
```

```
      if(time.gt.45 .and. time.le.105)then
       rstar1=2*a*time
       rstar2=2*a*(time-45)
       top1=r**2.-rstar1
       top2=r**2.-rstar2
       bot1a=alpha2*(rstar1**1.5)
       bot2a=alpha2*(rstar2**1.5)
       bot1b=diff2*(rstar1**2.0)
       bot2b=diff2*(rstar2**2.0)
       bot1=2*sqrt(bot1a+bot1b)
       bot2=2*sqrt(bot2a+bot2b)
       if(bot1.eq.0.0)bot1=.00000001
       if(bot2.eq.0.0)bot2=.00000001
       xa=top1/bot1
       xb=top2/bot2
       cest=.5*(c1-c0)*erfc(xa) + .5*(c2-c1)*erfc(xb) + c0
      endif

      if(time.gt.105)then
       rstar1=2*a*time
       rstar2=2*a*(time-45)
       rstar3=2*a*(time-105)
       top1=r**2.0-rstar1
       top2=r**2.0-rstar2
       top3=r**2.0-rstar3
       bot1a=alpha2*(rstar1**1.5)
       bot1b=alpha2*(rstar2**1.5)
       bot1c=alpha2*(rstar3**1.5)
       bot2a=diff2*(rstar1**2.0)
       bot2b=diff2*(rstar2**2.0)
       bot2c=diff2*(rstar3**2.0)
       bot1=2*sqrt(bot1a+bot2a)
       bot2=2*sqrt(bot1b+bot2b)
       bot3=2*sqrt(bot1c+bot2c)
       if(bot1.eq.0.0)bot1=.00000001
       if(bot2.eq.0.0)bot2=.00000001
       if(bot3.eq.0.0)bot3=.00000001
       xa=top1/bot1
       xb=top2/bot2
       xc=top3/bot3
       ca=c1-c0
       cb=c2-c1
       cest=.5*(ca)*erfc(xa) + .5*(cb)*erfc(xb) -
     /.5*(cb)*erfc(xc) + c0
      endif
      return
      end

c   Complimentary error function is given by Abramowitz
c     and Stegun (1972).
      function erfc(x)
```

```
a1=0.254829592
a2=-0.284496736
a3=1.421413741
a4=-1.453152027
a5=1.061405429
p=0.3275911
x1=abs(x)
t=1.0/(1.0+p*x1)
erf=1.0-(a1*t+a2*t**2+a3*t**3+a4*t**4+a5*t**5)*exp(-x1**2)
if(x.lt.0.0)erf=-erf
erfc=1.0-erf
return
end
```

LIST OF REFERENCES

Abramowitz, M., and I.A. Stegun, editors, 1972, Handbook of Mathematical Functions with Formulas, Graphs, and Mathematical Tables, U.S. Department of Congress, National Bureau of Standards, Applied Mathematics Series 55, 1046 p.

Barber, L.B. II, 1987, Influence of geochemical heterogeneity in a sand-and-gravel aquifer on the transport of nonionic organic solutes: methods of sediment characterization: in Franks, B.J., editor, U.S. Geological Survey Program on Toxic Waste--Ground-water Contamination: Proceedings of the Third Technical Meeting, Pensacola, Florida, March 23-27, 1987: U.S. Geological Survey Open File Report 87-109, pp. B47-B53.

Bear, J., 1972, Dynamics of Fluids in Porous Media: American Elsevier, 764 p.

Birch, A.F., J.F. Schairer, and H.C. Spicer, 1942, Handbook of Physical Constants: Geological Society of America Special Paper 36, 300 p.

Boyle, J.M., and Z.A. Saleem, 1979, Determination of recharge rates using temperature-depth profiles in wells: Water Resources Research, Vol. 15, No. 6, pp. 1616-1622.

Bredehoeft, J.D., and I.S. Papadopulos, 1965, Rates of vertical groundwater movement estimated from the earth's thermal profile: Water Resources Research, Vol. 1, No. 2, pp. 325-328.

Cartwright, K., 1970, Groundwater discharge in the Illinois Basin as suggested by temperature anomalies: Water Resources Research, Vol. 6, No. 3, pp. 912-918.

Davis, S.N., D.J. Campbell, H.W. Bentley, and T.J. Flynn, 1985, Groundwater Tracers: National Water Well Association, Worthington, Ohio, 200 p.

Deer, W.A., R.A. Howie, and J. Zussman, 1966, An Introduction to the Rock-forming Minerals: Longman Group Limited, London, 528 p.

Flynn, T.J., 1985, Water temperature as a groundwater tracer in fractured rock, M.S. Thesis, Department of Hydrology and Water Resources, University of Arizona, Tucson, Arizona, 67 p.

Freeze, R.A., and J.C. Cherry, 1979, Groundwater: Prentice-Hall, Englewood Cliffs, New Jersey, 604 p.

LIST OF REFERENCES--Continued

Garabedian, S.P., D.R. LeBlanc, K.M. Hess, and R.D. Quadri, 1987, Natural-gradient tracer test in sand and gravel: results of spatial moments analysis: in Franks, B.J., editor, U.S. Geological Survey Program on Toxic Waste--Ground-water Contamination: Proceedings of the Third Technical Meeting, Pensacola, Florida, March 23-27, 1987: U.S. Geological Survey Open File Report 87-109, pp. B13-B16.

Gelhar, L.W., and M.A. Collins, 1971, General analysis of longitudinal dispersion in nonuniform flow: Water Resources Research, Vol. 7, No. 6, pp. 1511-1521.

Hess, K.M., D.R. LeBlanc, and S.H. Wolf, 1987, Preliminary measurements of aquifer heterogeneity at a tracer test site, Cape Cod, Massachusetts: EOS, Vol. 68, No. 16, April 21, 1987, p. 299.

Hess, K.M., S.H. Wolf, D.R. LeBlanc, S.P. Garabedian, and M.A. Celia, 1987, Natural-gradient tracer test in sand and gravel: Preliminary results of laboratory and field measurements of hydraulic conductivity: in Franks, B.J., editor, U.S. Geological Survey Program on Toxic Waste--Ground-water Contamination: Proceedings of the Third Technical Meeting, Pensacola, Florida, March 23-27, 1987: U.S. Geological Survey Open File Report 87-109, pp. B25-B26.

Houpeurt, A., J. Delouvrier, and R. Iffly, 1965, Fonctionnement d'un doublet hydraulique de refroidissement: Memoires et Travaux de la Societe Hydrotechnique de France, No. 1, pp. 23-30.

Keys, W.S., and R.F. Brown, 1978, The use of temperature logs to trace the movement of injected water: Ground Water, Vol. 16, No. 1, pp. 32-48.

Lapham, W.W., 1987, Use of temperature profiles measured beneath streams to determine rates of vertical ground-water flow and vertical hydraulic conductivity: U.S. Geological Survey Water Resources Investigations Report 87-4054, 101 p.

LeBlanc, D.R., 1984, Sewage plume in a sand and gravel aquifer, Cape Cod, Massachusetts: U.S. Geological Survey Water-Supply Paper 2218, 28 p.

LeBlanc, D.R., J.H. Guswa, M.H. Frimpter, and C.J. Londquist, 1986, Ground-water resources of Cape Cod, Massachusetts: U.S. Geological Survey Hydrologic Investigations Atlas 692, 4 plates.

LIST OF REFERENCES--Continued

LeBlanc, D.R., 1987, Fate and transport of contaminants in sewage-contaminated ground water on Cape Cod, Massachusetts: in Franks, B.J., editor, U.S. Geological Survey Program on Toxic Waste--Ground Water Contamination: Proceedings of the Third Technical Meeting, Pensacola, Florida, March 23-27, 1987: U.S. Geological Survey Open File Report 87-109, pp. B3-B7.

LeBlanc, D.R., S.P. Garabedian, W.W. Wood, K.M. Hess, and R.D. Quadri, 1987, Natural-gradient tracer test in sand and gravel: objective, approach, and overview of tracer movement: in Franks, B.J., editor, U.S. Geological Survey Program on Toxic Waste--Ground-water Contamination: Proceedings of the Third Technical Meeting, Pensacola, Florida, March 23-27, 1987: U.S. Geological Survey Open File Report 87-109, pp. B9-B12.

LeBlanc, D.R., S.P. Garabedian, R.D. Quadri, R.H. Morin, W.E. Teasdale, and F.L. Paillet, in print, Hydrogeologic controls on solute transport in a plume of sewage-contaminated ground water, Cape Cod, Massachusettts; in Ragone, S.P., editor, U.S. Geological Survey Toxic Waste--Ground-water Contamination Program: Fiscal year 1986 program overview and selected abstracts from the October 21-25, 1985, technical review meeting, Cape Cod, Massachusetts: U.S. Geological Survey Open File Report 86-481.

Lunardi, V.J., 1981, Heat transfer in cold climates: Van Nostrand Reinhold Company, New York, New York, 731 p.

Marshall, T.J., and J.W. Holmes, 1979, Soil Physics: Cambridge University Press, Cambridge, England, 345 p.

Marsily, G. de, 1981, Storage in the ground: in G Beghi, editor, Thermal Energy Storage: D. Reidel Publishing Company, Dordrecht, Holland, p. 145-177.

Marsily, G. de, 1986, Quantitative Hydrogeology: Academic Press, Orlando, Florida, 440 p.

Miller, R.T., 1985, Preliminary modeling of an aquifer thermal-energy storge system: in S. Subitzky, editor, Selected Papers in the Hydrologic Sciences 1985: U.S. Geological Survey Water-Supply Paper 2270, p. 1-19.

Molz, F.J., A.D. Parr, P.F. Andersen, and V.D. Lucido, 1979, Thermal energy storage in a confined aquifer: experimental results: Water Resources Research, Vol. 15, No. 6, p. 1509-1514.

LIST OF REFERENCES--Continued

Norris, S.E., and A.M. Spiker, 1962, Temperature-depth relations in wells as indicators of semi-confining beds in valley-train aquifers: U.S. Geological Survey Professional Paper 450-B, pp. 103-105.

Oldale, R.N., 1976, Notes on the generalized geologic map of Cape Cod: U.S. Geological Survey Open File Report 76-765, 23 p.

Oldale, R.N., 1981, Pleistocene stratigraphy of Nantucket, Martha's Vineyard, The Elizabeth Islands and Cape Cod, Massachusetts: in Larson, G.J., and Stone, B.D., editors, Late Wisconsinian Glaciation of New England: Kendall/Hunt, Dubuque, Iowa, pp. 1-34.

Parr, A.D., F.J. Molz, and J.G. Melville, 1983, Field determination of aquifer thermal energy storage parameters: Ground Water, Vol. 21, No. 1, pp. 22-35.

Sauty, J.P., A.C. Gringarten, and P.A. Landel, 1979, The effects of thermal dispersion on injection of hot water in aquifers: Proceedings of Second Invitational Well Testing Symposium, Lawrence Berkeley Laboratory, Berkeley, California, pp. 122-131.

Sauty, J.P., A.C. Gringarten, H. Fabris, D. Thiery, A. Menjoz, and P.A. Landel, 1982, Sensible energy storage in aquifers, 2. Field experiments and comparison with theoretical results: Water Resources Research, Vol. 18, No. 2, pp. 253-265.

Schneider, R., 1972, Distortion of the geothermal field in aquifers by pumping: U.S. Geological Survey Professional Paper 800-C, pp. 267-270.

Sorey, M.L., 1971, Measurement of vertical groundwater velocity from temperature profiles in wells: Water Resources Research, Vol. 7, No. 4, pp. 963-970.

Stallman, R.W., 1963, Notes on the use of temperature data for computing ground-water velocity: in Methods of Collecting and Interpreting Ground-water Data, compiled by R. Bentall: U.S. Geological Survey Water-Supply Paper 1544-H, pp. 36-46.

Supkow, D.J., 1970, Subsurface heat flow as a means for determining aquifer characteristics in the Tucson basin, Pima County, Arizona, Ph.D. Dissertation, University of Arizona, Tucson, Arizona, 182 p.

Tsang, C.F., and D.L. Hopkins, 1982, Aquifer thermal energy storage: a survey: Geological Society of America, Special Paper 189, pp. 427-441.

LIST OF REFERENCES--Continued

Voss, C.I., 1984, SUTRA, Saturated-Unsaturated Transport: U.S. Geological Survey Water Resources Investigations Report 84-4369, 409 p.

Yellow Springs Instrument Company, 1985, Temperature, humidity, oxygen, pressure instruments, and sensors: Yellow Springs Instrument Company, Yellow Springs, Ohio, pp. 9-12.